Grain size sorting over offshore sandwaves

I.G.M. Wientjes

Supervisors:
Prof.dr. S.J.M.H. Hulscher
Ir. F.M. van der Meer
Dr.ir. P.C. Roos
Ir. J. van den Berg
Dr. T.A.G.P. van Dijk

July 2006

CE&M research report 2006R-004 / WEM-005
ISSN 1568-4652

Preface

This report is the result of my Master thesis of Civil Engineering at the University of Twente. The project was carried out within the department of Water Engineering and Management.

Because of the support I received which enabled me to bring this research to a good ending; I would like to thank some people.

First of all I want to thank the members of the committee; my daily supervisor Fenneke van der Meer, for always making time for me and never got tired of answering my questions or reading my work and who provided me with many good ideas for my research, Joris van den Berg for letting me work with his code and improving my understanding of numerical modelling, Pieter Roos for his good advises and many good discussions which I enjoyed much, Thaiënne van Dijk for providing the data and for very interesting input from a different point of view and Suzanne Hulscher for her interest in my research and for giving me the opportunity to finish my master thesis in a sociable group. The last half year I learned quite a lot from all of you; thank you!

Further I want to thank my room mates for providing a good working climate and everyone not mentioned above who contributed to this work.

The used data for this research were collected by the Geological Survey of the Netherlands (TNO) and the Directorate North Sea, Dutch Public Works and Water Management (DNZ-RWS) as part of the project "Eco-morphodynamics of the Seafloor", financed by Delft Cluster. This work will contribute to the EU INTERREG III B project MESH (Mapping European Seabed Habitats, http://www.searchmesh.net).

Table of contents

Abstract

Offshore sandwaves are rhythmic patterns on the bed of shallow seas. Because of their dimensions and migration rate, they can affect several human activities in these seas. For this reason, morphodynamic models are developed, to investigate and simulate sandwave dynamics. The sediment in the sand wave models is up till now assumed to be homogeneous. This means that the sediment consists of grains which all have the same grain size. Natural sediment however, exists of grains with different grain sizes, this is heterogeneous sediment. The transport of heterogeneous sediment is subject to different mechanisms than the transport of homogenous sediment and can thus influence the sand wave characteristics. It also may due to the grain size sorting patters over sand waves, which can be observed in nature. To account for the heterogeneity of the sediment a fractional calculation of the sediment transport is implemented in an existing sandwave model, in combination with a correction factor that accounts for the fact that grains in heterogeneous sediment do not act as when they are surrounded by grains of the same size. An active layer model preserves sediment continuity. The resulting model shows grain size sorting over sand waves. A coarsening trend towards the crest is found, which agrees with field observations, although the processes seem to be more extreme than in nature. In the sandwave trough the sediment remains mixed.

1. Introduction

On the bottom of sandy shallow seas, different rhythmic features occur. One kind of these wave-like patterns are offshore sandwaves. They have a wavelength, which is the length from crest to crest, of several hundreds of meters (figure 1.1). Their height is several meters and may reach to one third of the total water depth. Sandwaves can migrate several meters per year. For more information on sandwave characteristics and dynamics, see Németh (2003).

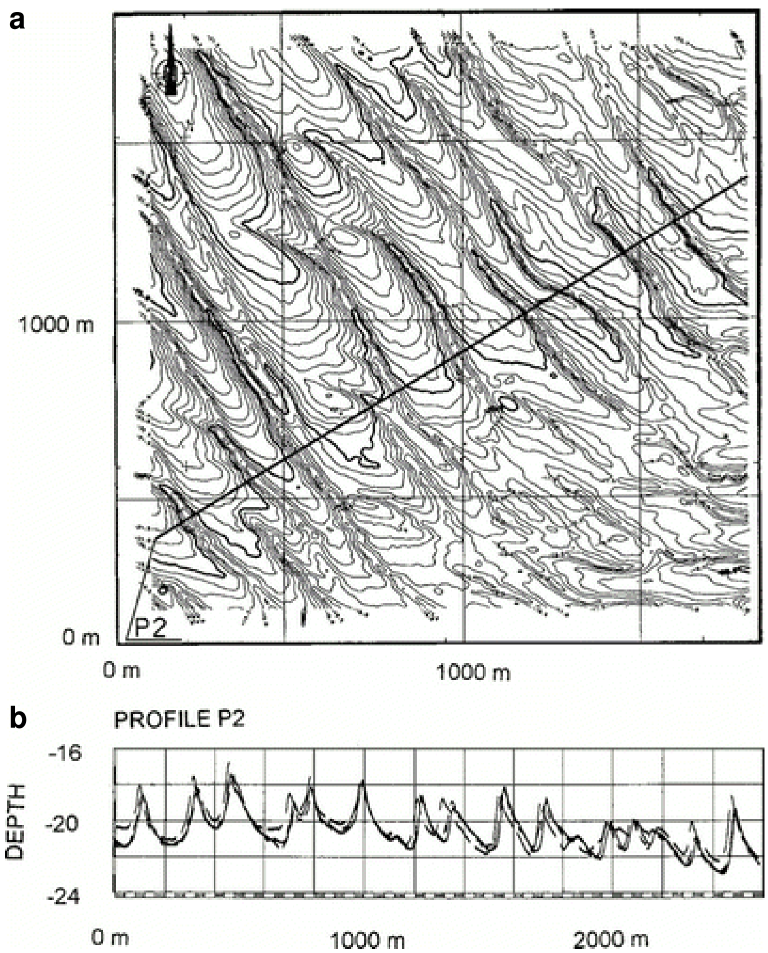

Figure 1.1: Sandwaves in the North Sea: (a) bottom topography; (b) bottom elevations along transect P2, measured in three different years (Blondeaux, 2001, adapted from Blondeaux et al 1999).

Because of their characteristics and behaviour, sandwaves can affect different human activities at the bottom in shallow seas. For instance, pipe lines or cables covered by a sandwave may become exposed to the water flow after sandwave migration, which can lead to their breaking or damaging. Another example are the shipping channels, were the depth can become too small for navigation when a sandwave migrates into such a channel. For a detailed overview how sandwaves can interfere with human activities in shallow seas, see Németh (2003).

Because of these problems, sandwave characteristics and behaviour are of practical relevance. To provide a better understanding of the offshore sandwaves, several models have been developed for sandwave investigation and simulation. One kind of these models is based on the idea of stability analyses. That means that the seabed and the water motion are considered as a dynamically coupled system, where the sandwaves developed as free instabilities of the system (for details see Appendix 1). Over the sandwaves, residual flow circulations appear in the water column, which induces a net sediment flux towards the sandwaves crest, which favours the sandwave development (Hulscher 1996).

Till now, sandwave simulation models are based on the assumption of homogeneous sediment. That is sediment that consists of grains with only one size. Natural sediment however, consists of particles with many different grain sizes. When implementing heterogeneous sediment in a model, the model becomes more realistic and may give a better prediction of the sandwave characteristics and behaviour. McCave (1971) already assumed that the distribution of sediment sizes on a sandwave could account for the shape of asymmetrical types (figure 1.2). Németh (2003) also recommended investigation of the impact of the sediment characteristics, to provide a better insight in the mechanisms of sandwave development. Field observations also reveal grain size sorting over a sandwave (Tobias, 1989). With grain size sorting the spatial variation of grain sizes over a sandwave is meant. The sorting of grains can be interesting for practical purposes like sand extraction, if requirements exist on the grain size of the sediment that would be extracted (Németh, 2003).

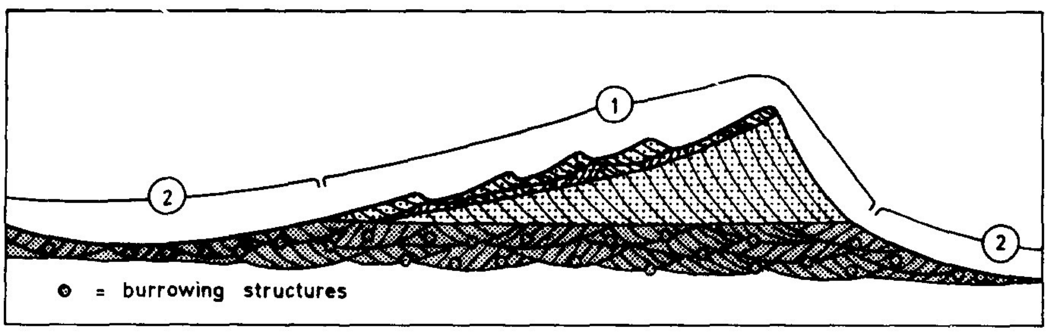

Figure 1.2: Hypothetical internal sedimentary structure of a sandwave with megaripples from McCave (1971). Zone 1 contains coarser sand and zone 2 contains finer sand.

The aim of this project is to provide a better understanding of the grain size sorting over sandwaves, by including the relevant processes for heterogeneous sediment in an existing morphodynamic model.

The research questions are:

- When implementing heterogeneous sediment in an existing sandwave model, can this model make grain size sorting visible?
- If this is possible, how are the grains sorted over a sandwave?
- What is the influence of heterogeneous sediment on sandwave characteristics, compared with homogeneous sediment?
- Does the model results agree with the grain size sorting observed in nature?

To answer these questions, knowledge is required about the relevant processes of grain size sorting. In chapter 2 an inventory is made of the research that is already done on grain size sorting over the flat bed and bedforms other than sandwaves. In chapter 3 some background information about sediment is given. To compare the model results with nature, insight in grain size sorting observed in nature is necessary. Therefore in chapter 4 some analysis is given from data from TNO, of sediment samples on sandwaves. Chapter 5 deals with the used model. Also the adaptations which are made to the model, to make it work for heterogeneous sediment, are explained in this chapter. In chapter 6 the results obtained with this extended model are given. Chapter 7 discusses these results. Finally, chapter 8 and 9 give the conclusions and recommendations.

2. Actual knowledge of grain size sorting

No detailed research about the mechanisms of grain size sorting over sandwaves has been carried out yet. However, sorting processes on bedforms different from sandwaves have been investigated. In the first section of this chapter, the main effects of the heterogeneous sediment are briefly mentioned. In the next section, some model results for grain size sorting over bedforms are discussed, to provide an understanding of the possible influence of heterogeneous sediment.

2.1 Behaviour of heterogeneous sediment in general

The presence of heterogeneous sediment may result in processes of grain-size sorting for both the flat bed and bedforms.

A bed can be covered with a coarse bed layer. This armour layer (or mobile pavement) can develop if a significant amount of coarse material is not or barely transported by the flow. Also the winnowing or washing out of fine grains from between and below the coarse material, contributes to the formation of a coarse bed layer (Blom, 2003).

For different types of bedforms, different types of sorting can be observed. In river dunes the coarse size fractions are mainly found in the lower parts of the bedforms. This results from the avalanching of grains down the bedform lee face (Blom, 2003). The mechanisms that cause this downward coarsening are specific for unidirectional flow condition (rivers). As the here investigated sandwaves are bedforms under tidal conditions (shallow seas), this mechanisms will not be discussed in detail.

Grain size sorting over bedforms in shallow seas can also be observed. For these tidal bedforms often a coarsening trend from the trough towards the crest occur. This can be a result of the large flow velocity near the crest, which washes away the finer grains from the crest, leaving the coarser grains behind. Finer grains accumulate at the troughs where flow velocities are smaller. Different investigation is done about this kind of grain size sorting over bedforms. The results of these researches will now be discussed.

2.2 State-of-the art of morphodynamic modelling for heterogeneous sediment

The studies that now are discussed, are based on morphodynamic models which are solved using a linear stability approach (see Appendix 1). The effects of heterogeneous sediment are modelled using bimodal sediment (sediment with only two grain sizes, see also chapter 3.3), a fractional calculation with a correction factor to account for the influence of other fractions and an active layer model to preserve sediment continuity.

Foti and Blondeaux (1995) investigated the effect of mixed sediment on sea ripple formation with both experiments and a theoretical model. Their experimental results show that the presence of mixed sediment tends to stabilize the bottom and causes longer ripples to appear. Their theoretical model shows sediment transport which tends to accumulate the coarse grains at ripple crests and leaving the fine ones in the troughs, in accordance with the experimental results. Good agreement was found between experimental data and theoretical findings.

Walgreen et al. (2003) developed a model to study the initial formation of shoreface-connected ridges on storm dominated shelves. Within their model, they considered both bed load and suspended load sediment fluxes to analyze the corresponding grain size distribution. They found a net stabilizing effect of sediment sorting on the growth of the bedforms. Due to the sediment mixture the growth rates decrease and the migration rates increase. The preferred wavelength becomes longer, although the wavelengths are only slightly affected by the sorting processes. The model shows also grain size sorting. The coarsest material occurs on the landward (up current) flank and the finer on the seaward (down current) flank of the ridges.

Walgreen et al. (2004) developed a model to analyze the effect of graded sediment on the formation of tidal sand ridges. Due tot the graded sediment the growth and migration rates increases, whereas the wavelength remains unchanged. Under M_2 tidal conditions, the coarser grains accumulated at the crest. Adding an M_4 tidal constituent or a steady current to the forcing, results in a coarser landward flank.

Lanzoni and Tubino (1999) used a two-dimensional model to investigate the effect of mixed sediment on the development of alternate bars. Although this type of bedforms occurs in streams and rivers, they show the same coarsening trend towards the bar crests as the tidal bedforms and therefore they are mentioned here. They found that heterogeneous sediment leads to a reduction of growth rate and migration rate of the bars. Furthermore, they found that the bar wavelength is shortened with respect of the case of uniform sediment.

When comparing these investigations, it can be said that the grain sorting on bedforms caused very different effects on the wavelengths, the growth rate and the migration rate for different types of bedforms. Table 1.1 summarizes these effects. The different results may be caused by different model assumptions or by the physics of the different bedforms.

	Length	**Growth rate**	**Migration rate**	**Grain size sorting trend**
Sea ripples	Longer	Decrease	-	Coarsening trend towards crest
Shoreface-connected ridges	Slightly longer	Decrease	Increase	Coarsening trend towards landward flank
Tidal sand ridges	Unchanged	Increase	Increase	Coarsening trend towards crest or landward flank
Alternate bars in rivers	Shorter	Decrease	Decrease	Coarsening trend towards the crests

Table 2.1: Different results from investigation of grain size sorting over bedforms.

3. Sediment characteristics

Before something can be said about the transport of heterogeneous sediment, knowledge is required about the sediment itself. Therefore some background information about sediment is given in this chapter.

3.1 Sediment

Sediment properties such as density, size, gradation and cohesion, can influence the sediment transport. In this study, the material is supposed to be no cohesive (sand and gravel). The density of natural sediments is approximately equal to 2650 kg/m^3 (Soulsby, 1997). Natural sediment consists of particles with different grain sizes. Names for this are mixed, graded, non-uniform or heterogeneous sediment. The size of a particle can be expressed by its diameter, D. Since natural sediment particles are not precisely spherical, the “diameter” cannot be determined by simply measuring it. Therefore for coarse particles, D is often defined as the dimension of the smallest mesh opening through which the particle will pass, and for finer particles as the diameter of the equivalent sphere with the same fall velocity as the actual particle (Parker, 2005). Usually the material is classified in size-classes on the basis of the diameter. Sand for instance has grain diameters in the range 0.0625mm to 2mm according to the Udden-Wentworth scale (Soulsby, 1997).

3.2 Continuous grain size distribution

The grain sizes of sediment have a continuous distribution. This distribution is usually presented as a cumulative curve showing the percentage by mass of grains smaller than D, versus D. See figure 3.1 for an example of such a cumulative curve. The grain sizes are denoted as D_n. This indicates the grain diameter for which n% of the grains by mass is finer (Soulsby, 1997).

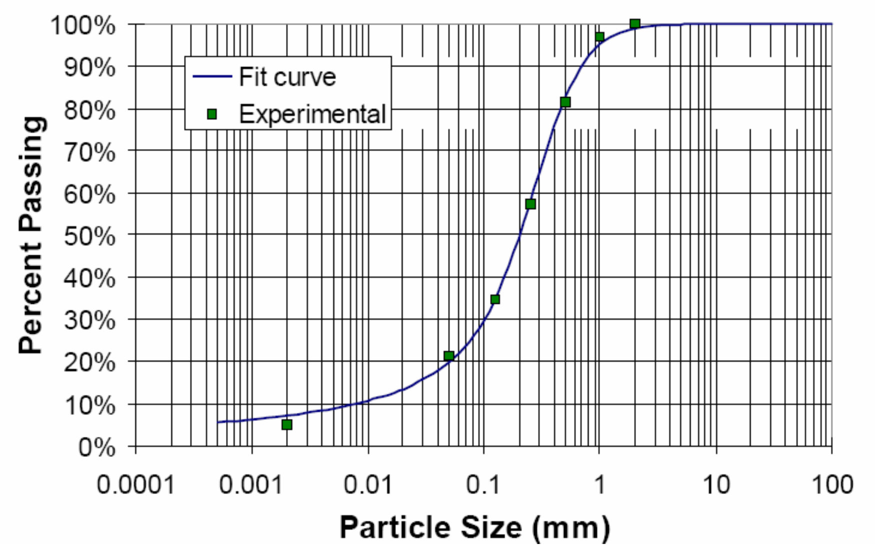

Figure 3.1: Cumulative grain size curve.

The probability density function $F(D;\ \mathbf{x},t)$ describes the distribution of grain sizes. Hereby $F(D;\ \mathbf{x},t)dD$ gives the concentration of a volume sample taken at position **x** and time t, consisting of particles with sizes falling in the range $D,\ D+dD$. The probability, p, that there are grains in a sediment sample between the values a and b is:

$$p\left[a \le D \le b\right] = \int_a^b F dD \,. \qquad (3.1)$$

It must satisfy the constraint $\int_0^\infty F dD = 1$.

Some definitions can be used to describe the distribution of the sediment.
The median grain size, D_{50}, is the midpoint of a distribution, that means that 50% of the grains is larger and 50% is smaller than this value. The mean grain size, D_m can be expressed as:

$$D_m = \int_0^\infty D F dD \,. \qquad (3.2)$$

If the grain sizes have a normal distribution, the mean size equals D_{50}. This is however not so for a skewed distribution.

The standard deviation σ, or variance σ^2, can be calculated from:

$$\sigma^2 = \int_0^\infty \left(D - D_m\right)^2 F dD \,. \qquad (3.3)$$

This gives some measure of the spread of the sediment distribution.

3.3 Grain size classes

Sediment can be divided into classes or fractions. The equation for the mean grain size becomes:

$$D_m = \sum_{i=1}^{N} F_i D_i \,, \qquad (3.4)$$

in which the probability F_i is the percentage (between 0 and 1) at which a certain grain size is present in the material, D_i is the grain size of this fraction i and N the number of classes (or fractions) in which the material is divided.

The standard deviation σ (or variance σ^2) becomes:

$$\sigma^2 = \sum_{i}^{N} F_i (D_i - D_m)^2 \,. \qquad (3.5)$$

For the modelling of the heterogeneous sediment in this research, also grain size fractions are used. For simplicity a bimodal mixture is chosen. That is a sediment mixture that consists of only two grain sizes. In figure 3.2 the cumulative grain size distribution of bimodal sediment is shown.

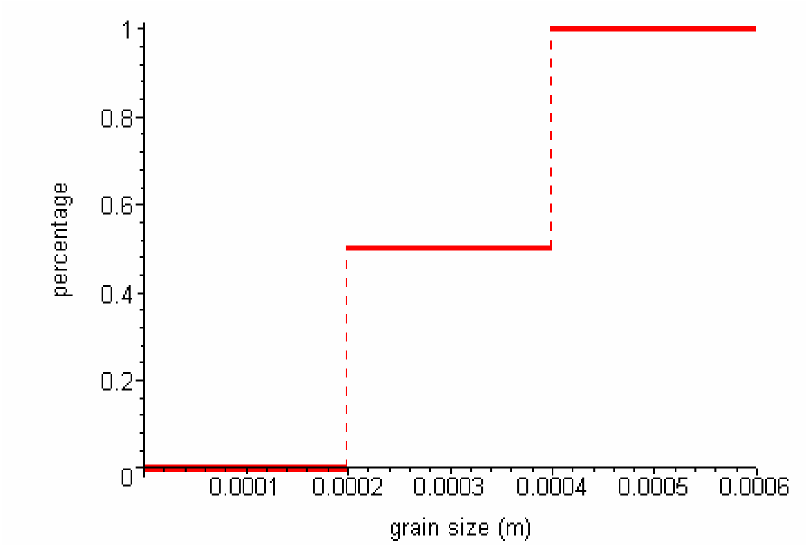

Figure 3.2: Cumulative grain size curve for a bimodal sediment mixture, consisting of 50% sediment of 200 μm and 50% of 400 μm.

3.4 Normal and log-normal grain size distribution

Sediment can have a normal distribution, but often the distribution of the grains is skewed. It is widely accepted that many mixed sediments have a grain-size distribution that approximates a log-normal distribution; that is, the logarithm of the grain size has an approximately normal (Gaussian) frequency distribution by weight. (See figure 3.1 where a logarithmic scale for the grain size is used.) Often therefore the phi-scale (a base-2 logarithmic scale) is used for grain sizes (Soulsby, 1997). For D in mm it is defined as:

$$D / D_{ref} = 2^{-\phi} \text{ with } D_{ref} = 1 \text{ mm}, \tag{3.6}$$

$$\phi = -\log_2 (D / D_{ref}) = -\frac{\ln(D / D_{ref})}{\ln(2)}. \tag{3.7}$$

This ϕ then has a normal grain size distribution. Now the probability density function becomes $F(\phi;\ \mathbf{x},t)$. Hereby $F(\phi;\ \mathbf{x},t)d\phi$ gives the concentration of a volume sample taken at position **x** and time t, consisting of particles with sizes falling in the range $\phi, \phi+d\phi$. It must satisfy the constraint:

$$\int_{-\infty}^{\infty} F d\phi = 1 \qquad (\sum_{i=1}^{N} F_i = 1).$$

F_i is the probability of the grain-size class i. The mean (or average) value ϕ_m and the variance σ^2 (standard deviation σ) becomes in phi-terms (Soulsby, 1997):

$$\phi_m = \int_{-\infty}^{\infty} \phi F d\phi \quad (\ \phi_m = \sum_{i=1}^{N} \phi_i F_i), \tag{3.8}$$

$$\sigma^2 = \int_{-\infty}^{\infty} (\phi - \phi_m)^2 \, F d\phi \quad (\sigma^2 = \sum_{i=1}^{N} (\phi - \phi_m)^2 \, F_i). \tag{3.9}$$

These equations provide an understanding of the grain size distributions.

4. Data

For this project grain size data from TNO are available, from 3 different sandwave areas in the North Sea. One area is located on a shoreface-connected ridge near Zandvoort and another area in a sandwave field 50 km offshore, see also figure 4.1 (Van Dijk, 2002). The data of these areas were collected in March 2001. The third area is also offshore and lies 45 km west of Hoek van Holland (figure 4.2) and the data from this area were collected in April 2001. For this research the data is investigated to see whether grain size sorting on sandwaves occurs in reality. In this section the results of this will be discussed for the different areas.

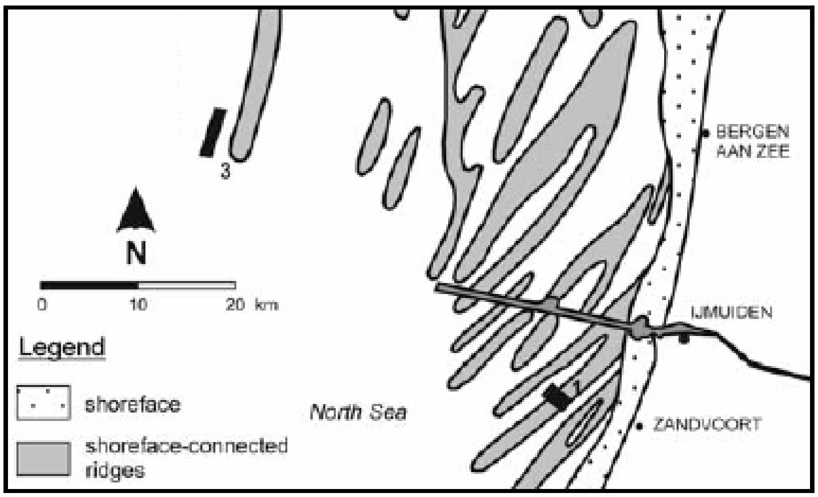

Figure 4.1: Location map of two sampling sites in the North Sea: 1. lower shoreface with shoreface-connected ridges; 3. sandwave field 50 km offshore (Van Dijk, 2002).

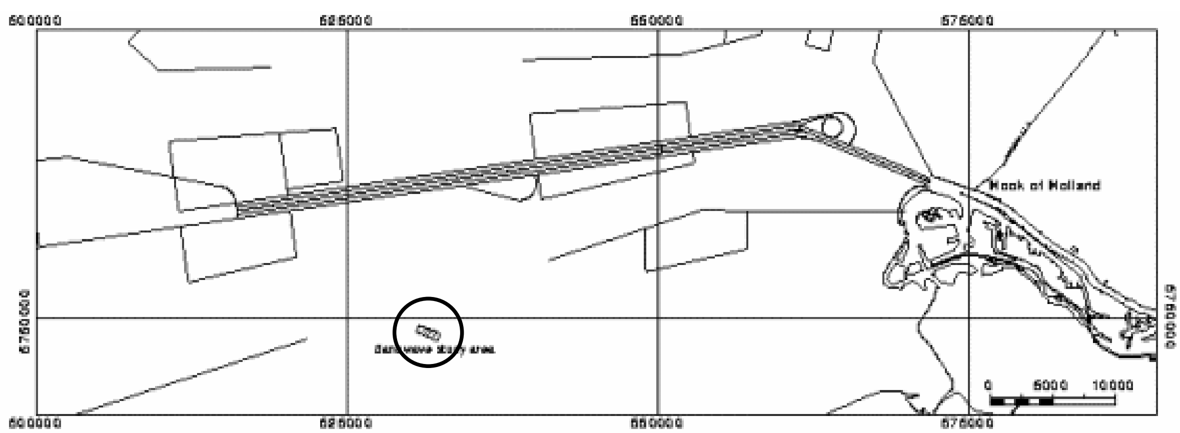

Figure 4.2: Sandwave study area (encircled in the figure), 45 km west of Hoek van Holland, scale in meters.

4.1 sandwaves on shoreface-connected ridge near Zandvoort

In this area samples are taken over three-dimensional compound sandwaves, with superimposed megaripples, on top of a shoreface-connected ridge, their lee sides facing north-northeast. The samples were taken from two of these sandwaves, with only the northern sandwave fitting entirely within the area of data collection (figure 4.3). This sandwave has a wavelength of 760 m and a height (difference between the flat-topped crest plateau and the adjacent troughs) of 1.5 m. For further details see Van Dijk and Kleinhans (2005) or Van Dijk (2002).

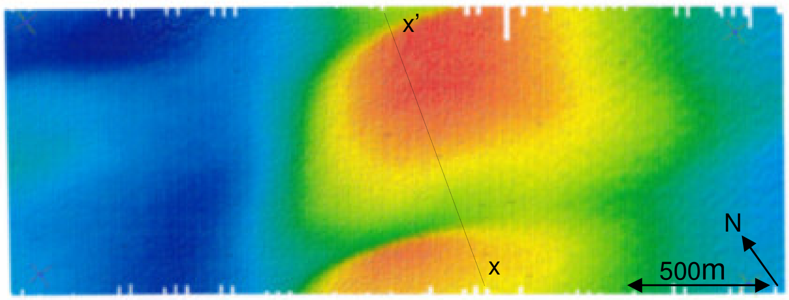

Figure 4.3: Multibeam echo image of the coastal site near IJmuiden in March 2001, showing large three-dimensional compound sandwaves on top of a shoreface-connected ridge (Van Dijk and Kleinhans, 2004).

In this figure 4.3 the darkest colour blue indicates the largest (18.3 m) depth and the colour red indicates the smallest (14.0 m) depth. The sandwaves are strongly asymmetrical in cross section, see figure 4.4.

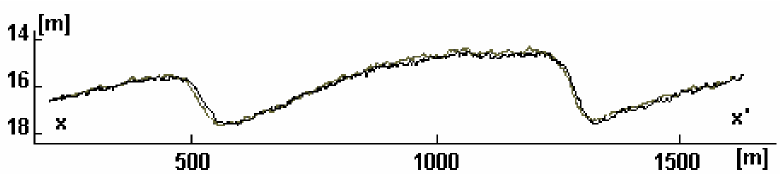

Figure 4.4: Cross-section of the sandwaves from figure 6 (Van Dijk and Kleinhans, 2004).

During the survey, the seabed was sampled using a cylindrical box corer. The analysis method for the grain sizes (smaller than 2 mm) was laser diffraction, using a Malvern 2000 (Van Dijk and Kleinhans, 2005). The grain size distributions are slightly skewed and therefore only near-normal (Van Dijk and Kleinhans, 2004). This can be seen from figure 4.5.

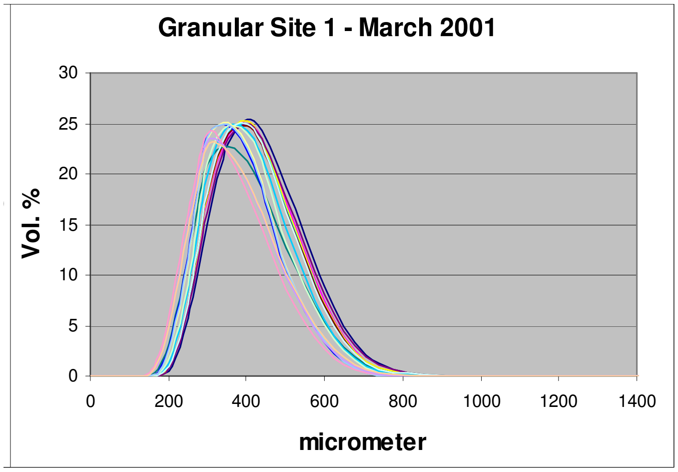

Figure 4.5: Grain size distribution of different located samples on the sandwaves on a shoreface-connected ridge.

From this survey, data of grain size samples (D_{10}, D_{50}, D_{60}, D_{90}) on different sampling points are available (Appendix 2). For each sample a uniformity coefficient (D_{60} / D_{10}) is calculated. When sediment is sorted over a sandwave, grains with the same sizes group together. Due to this, on locations of the sandwave a larger percentage of the grains fall within a certain grain size range, then in the case of no sorting. The uniformity coefficient of the sediment on such a location will be close to 1. When sediment is not sorted over the sandwave, on each location a broad range of different grain sizes will be present, causing a larger uniformity coefficient. To look only at the uniformity coefficient however, is not sufficient, because when in the whole sandwave area only grains within a small range of grain sizes are available, the uniformity coefficient will also be close to 1. Therefore it is necessary to look additionally whether the grain size differs for different sampling points. In figure 4.6 the uniformity coefficient is plotted against the median grain size (D_{50}) of the same sample location. Groups are made of the samples on the same morphological location of the sandwave. Note that the axes do not start with zero. See also Passchier and Kleinhans (2005).

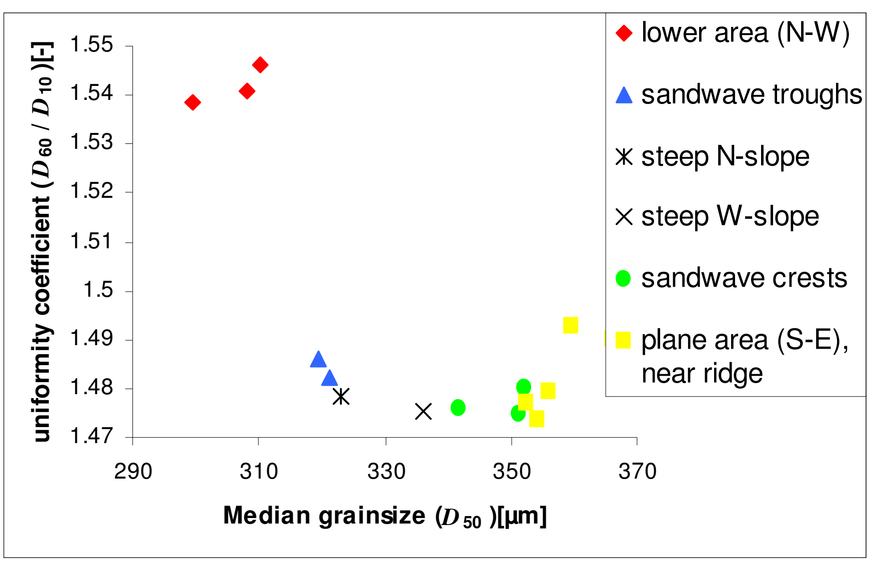

Figure 4.6: Sorting (D_{60}/ D_{10}) and median grain size (D_{50}) in µm for the sandwaves on a shoreface-connected ridge, (axes do not start with zero); reproduced after Passchier and Kleinhans (2005).

The uniformity coefficient of the sediment samples from the sandwaves and the plane area near the sandwaves, lies closer to 1 than those from the lower located area. The sandwave samples have also greater median grain sizes than in the lower area. This is indicates that larger grains have been transported from the lower area to the sandwaves on top of the ridge. Also, the grain size samples on the sandwave crest have some lager median grain sizes than those in the troughs (about 30 μm). The sampling points on the two slopes are located between crest and troughs. Their median grain sizes also lies between the crest and trough values. Therefore a coarsening trend from the through towards the crests seems to be apparent.

4.2 Sandwave field in offshore area

This area was sampled during the same survey as the area described in the previous section. In this offshore area there is a sandwave field of nearly two-dimensional compound sandwaves. See figure 4.7. In this figure again the darkest colour blue indicates the deepest and the colour red indicates the shallowest parts. The sandwaves have an average wavelength of 200 m and an average wave height of 1.8 m. For more information see Van Dijk and Kleinhans (2005) or Van Dijk (2002).

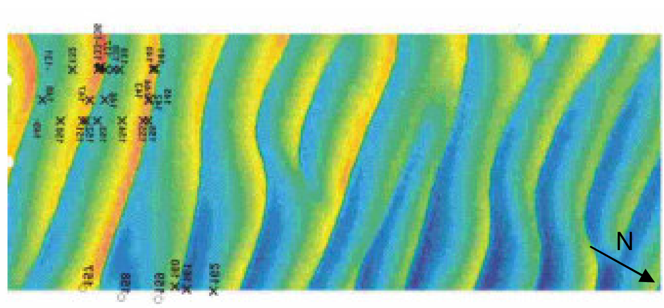

Figure 4.7: Multibeam echo image of the sandwave area 50 km offshore to the north-west of IJmuiden in March 2001, showing asymmetrical, two–dimensional compound sandwaves.

The sandwaves are in their cross-sectional profile less asymmetric than those in the area described in the previous section. Most of them are sharp-crested, but there are also a few rounded (figure 4.8). Their lee slopes face north. Their stoss sides, and for the rounded ones also the lee sides, are covered with megaripples (Van Dijk and Kleinhans, 2005 or Van Dijk, 2002).

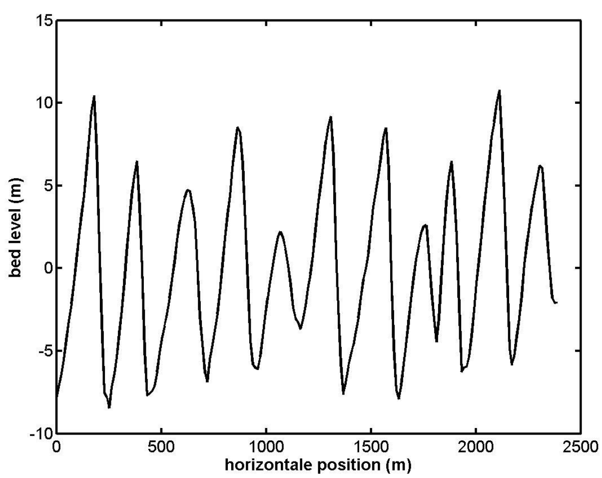

Figure 4.8: Cross-section through sandwave field from figure 10, on the topmost border.

In this area the measurement methods were as described in the previous section. In this case the grain size distributions are also near-normal but slightly skewed (Van Dijk and Kleinhans, 2004). This can be seen from figure 4.9.

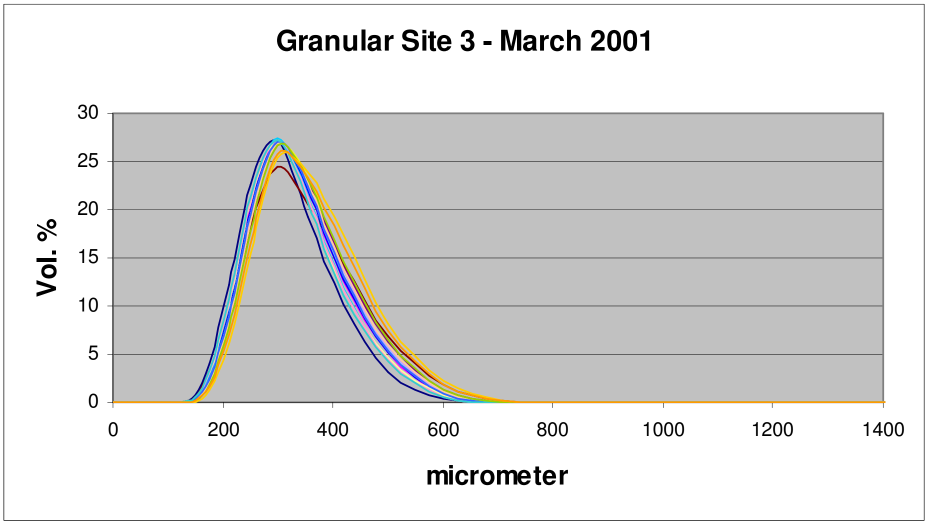

Figure 4.9: Grain size distribution of samples from the sandwave field in offshore area.

From this expedition, the same kind of grain size data (D_{10}, D_{50}, D_{60}, D_{90}) is available (Appendix 3). The samples were taken on sandwaves as well as on the megaripples. For this research only the sandwave samples are taken into account. Again the uniformity coefficient (D_{60}/ D_{10}) is calculated for each sample. In figure 4.10 this coefficient is plotted against the median grain size (D_{50}) of the same sample location. Two groups have been distinguished, sandwave crests and sandwave troughs. Note that the axes do no start with zero. See also Passchier and Kleinhans (2005).

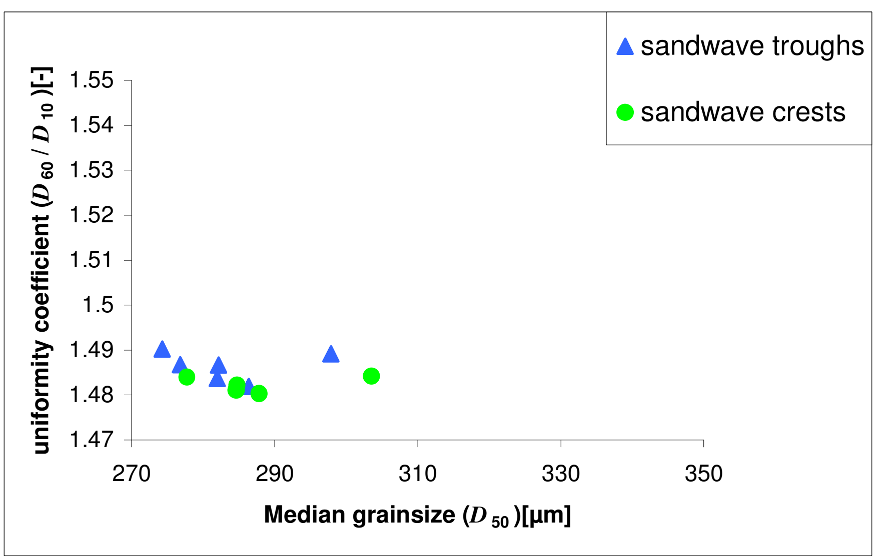

Figure 4.10: Sorting (D_{60}/ D_{10}) and median grain size (D_{50}) in µm for the sandwave field in offshore area, (axes do not start with zero); reproduced after Passchier and Kleinhans (2005).

This figure shows for both crests and troughs, median grain sizes scattered between 275 and 305 µm. For the uniformity coefficient, it can be said that the grain samples on the crest seems to be a little bit closer to 1 than those in the troughs. This difference however is negligible compared with the difference in uniformity coefficient from the samples from the sandwaves on the shoreface connected ridge (described in the previous section). No sorting trend is visible from this data. This agrees with the results of Van Dijk and Kleinhans (2004) and (2005) on the same data.

4.3 Sandwave field, 45 km west of Hoek van Holland

In this area a section of one sandwave was selected for surveying and studying. This sandwave is situated 45 km WSW of Hoek van Holland, about 12.5 km south of the main shipping channel to the Rotterdam harbour. The water depth above its crest is 20 to 24 m. The sandwave height is between 4.5 and 7 m. This sandwave section is part of a group of sandwaves that shows curved and bifurcating crest lines. This sandwave is rather stable (Schüttenhelm, 2002). As shown in figure 4.11, this sandwave is covered with other bedforms.

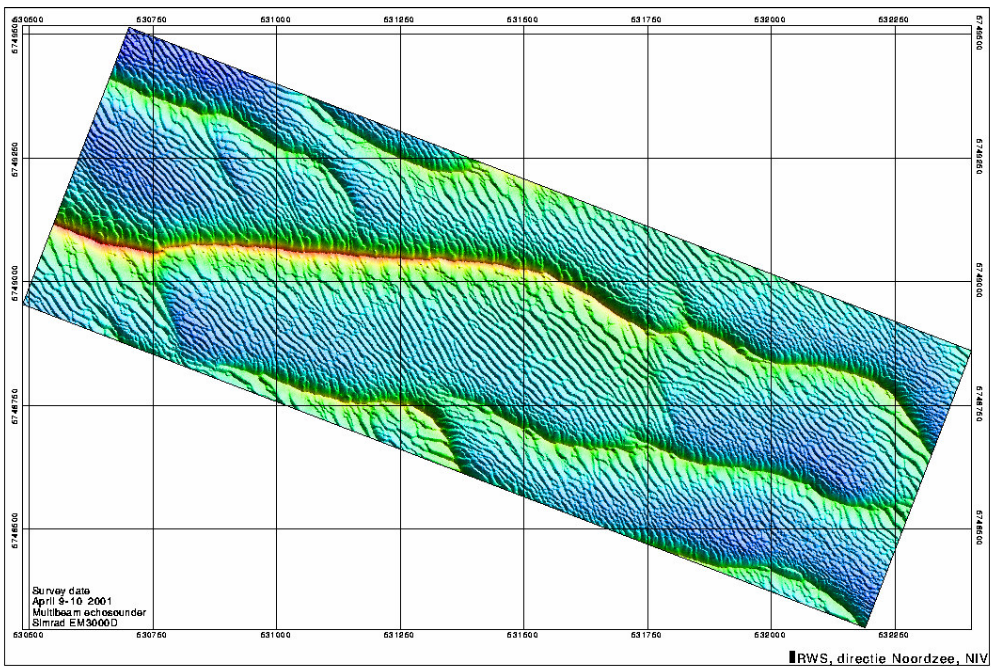

Figure 4.11: Multibeam bathymetric map of the study area, distances in meters.

In this area several vibrocores where taken (Schüttenhelm, 2002). For the analysis of grain sizes, again a Malvern 2000 is used (for grains < 2 mm). The samples were taken in April 2001, at three depths below the seabed for each sampling location. As can be seen from figure 4.12, there is a row of sampling points following the sandwave crest and there are two rows of sampling points perpendicular to the sandwave crests. For the samples of these last two rows, the median grain size, D_{50}, and the accompanying water depth are plotted against the sample locations, in figure 4.13. For the data see Appendix 4.

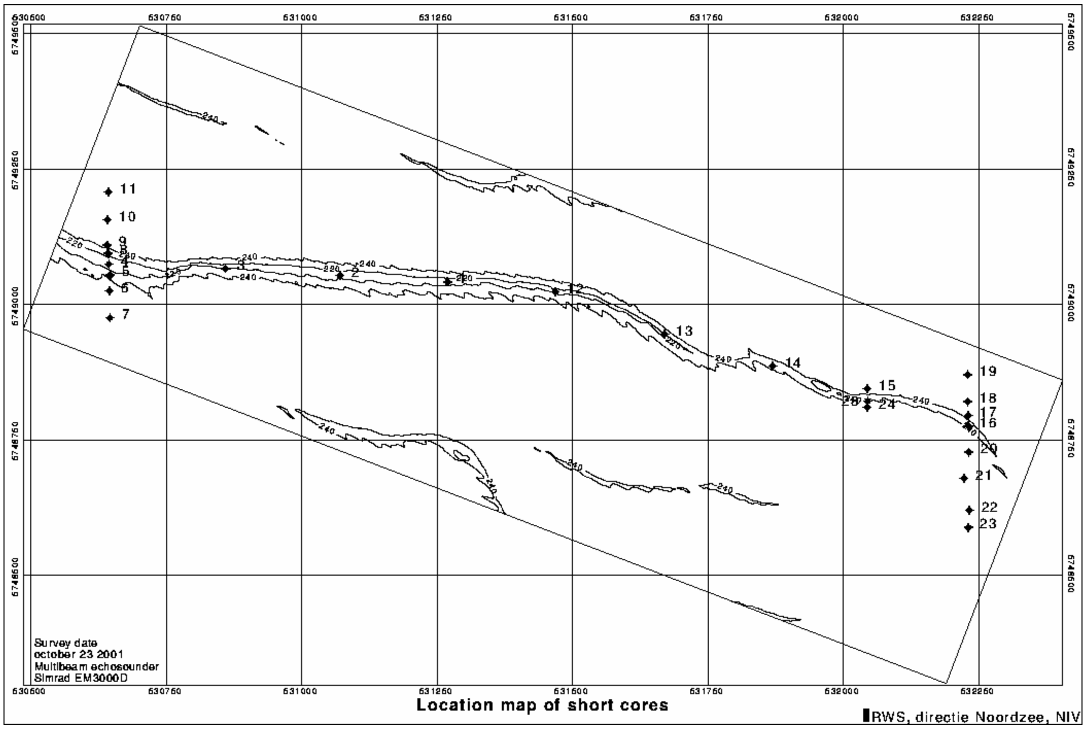

Figure 4.12: Detailed location map of the short cores within the area of study, horizontal scale in meters, bathymetric values in decimetres.

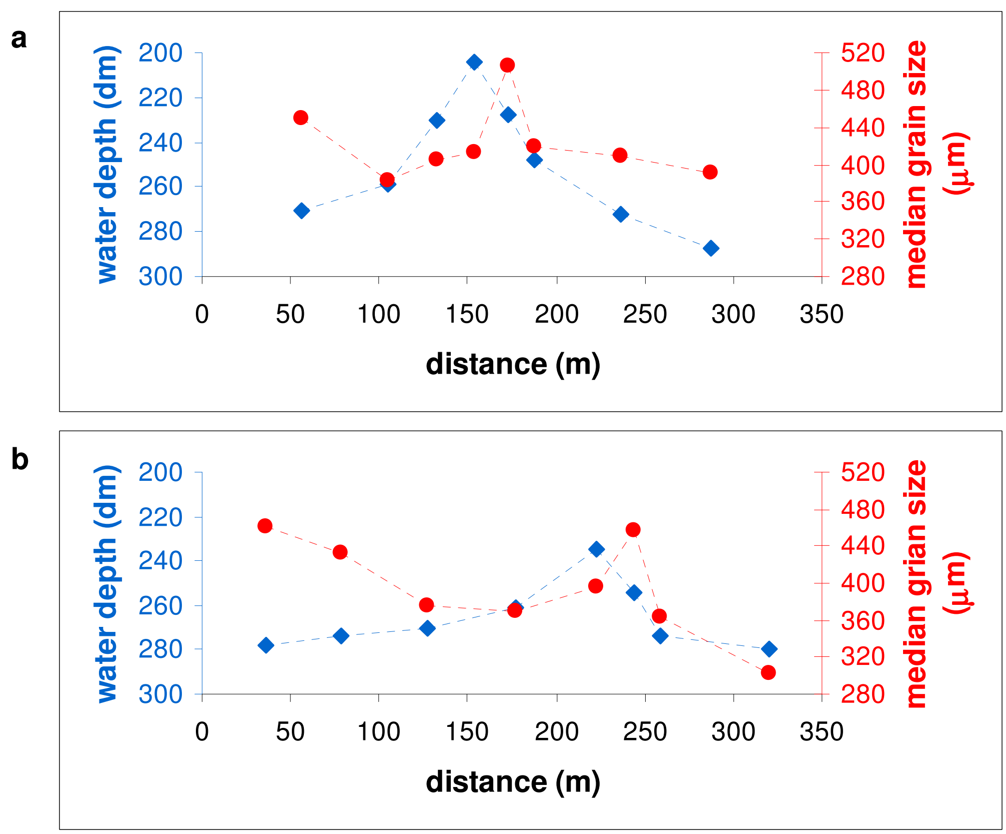

Figure 4.13: Water depth in dm and median grain sizes (D_{50}) in µm against the cross-section over the sandwave: (a) left cross-section (points 7-6-5-4-8-9-10-11); (b) right cross-section (points 23-22-21-20-16-17-18-19).

As can be seen from figure 4.13, the median grain sizes of the samples on the lower parts of the sandwave, the troughs, are smaller than the median grain sizes from the higher located part, the crest. This trend indicates sorting over the sandwave. The first left point in the figure 4.13a and the first left two points in figure 4.13b however, have relative large median grain sizes, although they are located on the sandwave trough. These sampling points are rather far away from the sandwave and could possible be influenced by the neighbour sandwaves.

Further, in both graphs there is a deviant point, with a relatively large median grain size. These two points lay on the eastern slope near the crest of the sandwave. When comparing the median grain sizes from this area with the ones of the areas from the previous sections, a difference is that the grain sizes in this area are larger. Possible, the grain characteristics influenced the occurrence and the trend of the sorting.

5. The mophodynamic model

For the simulation of grain size sorting, an existing model for tidal sandwaves is extended with equations for heterogeneous sediment. In the first section of this chapter the model for homogeneous sediment is described. In the following sections the adaptations to this model, to include the effects of heterogeneous sediment, are explained.

5.1 Actual model in the homogeneous sediment case

As mentioned in chapter 1, a stability approach can be used to model sandwaves. See also Appendix 1. A linear stability analysis can be used to solve the physical processes semi-analytically, gaining a good insight in the physical processes (Hulscher, 1996). However, due to this linearization, only the initial behaviour of the bedforms can be simulated. For this reason a non-linear simulation model has been developed to investigate the evolutionary processes of sandwaves after their initial evolution (Németh, 2003). A new code for this model is written by Van den Berg and Van Damme (2005). In this research the numerical code of Van den Berg is used to investigate the intermediate term behaviour of sandwaves.

The model describes the interaction between the tidal flow and the topography. The water motion causes sediment transport. Due to this transport, the sea bed evolves, which in turn affects the flow. This is called a morphodynamic loop (see figure 5.1). Because the bed topography changes on a timescale of years, whereas the tidal flow changes on a much smaller timescale, the bottom can be assumed to be constant during the flow calculation. Therefore, the model consists of two separated parts, one describing the flow and the other part describing the sediment dynamics. Now, first the part describing the flow is discussed, after which the sediment calculation is described.

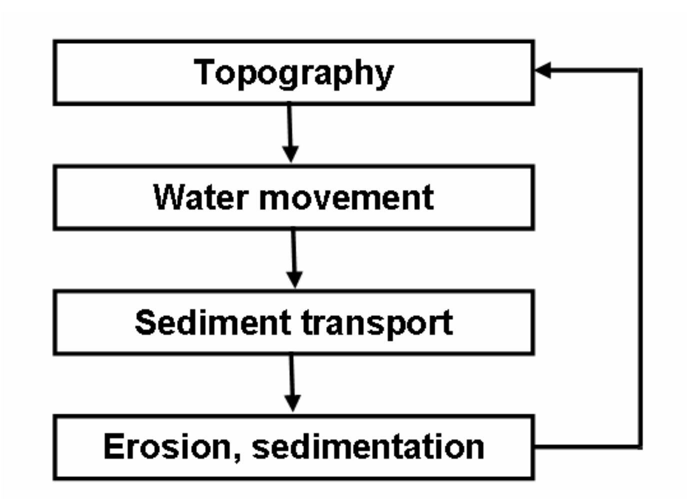

Figure 5.1: The morphodynamic loop, after Németh (2003).

5.1.1 Water motion

Because the Coriolis force only slightly affects sandwaves, the tidal flow can be described with the two-dimensional, vertical (2DV) shallow water equations (Németh, 2003). Standard incompressible hydrostatic equations are used, which are discussed in Van den Berg and Van Damme (2005):

$$\frac{\partial u}{\partial t}+u\frac{\partial u}{\partial x}+w\frac{\partial u}{\partial z}=A_v\frac{\partial^2 u}{\partial z^2}-g\frac{\partial \zeta}{\partial x}+F(t)\,, \tag{5.1}$$

$$\frac{\partial u}{\partial x}+\frac{\partial w}{\partial z}=0\,. \tag{5.2}$$

Here *u* and *w* are the flow velocities in respectively the horizontal (*x*) and vertical (*z*) directions, *g* (m/s^2) is the gravitational acceleration, *h*(m) the bed level with respect to the mean topography and ζ (m) is the water surface elevation relative to the mean free surface elevation $z = H$ (figure 5.2). A_v (m^2/s) is the vertical eddy viscosity and represents the fluid resistance, to changes in the horizontal velocity, in the vertical direction. Time is denoted by t. The term $F(t)$ (m/s^2) is used to mimic the tidal forcing and is composed of three components (F_0, F_s and F_c):

$$F(t)=F_0+F_s\sin(\omega t)+F_c\cos(\omega t)\,, \tag{5.3}$$

with ω (1/s) the angular frequency For more information about the tidal forcing calculation, see Van den Berg and Van Damme (2005).

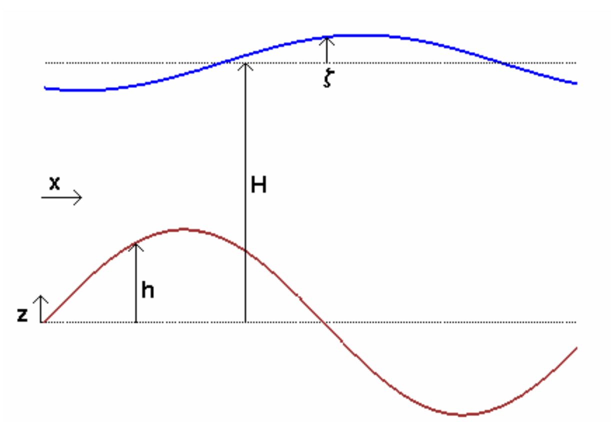

Figure 5.2: Situation sketch. The average height of the water column is H, h(x) is the bottom height and ζ(x,t) the surface elevation.

Models that use only a horizontally independent eddy viscosity formulation and no-slip condition tend to overestimate the bed shear stress (equation (5.8)). Therefore a partial slip condition on the bottom is needed. This partial slip condition describes the horizontal flow components:

$$A_v\frac{\partial u}{\partial z}=Su\bigg|_{z=h(x)}\,. \tag{5.4}$$

S (m/s) is the resistance parameter controlling the shear stress at the seabed. When S = 0, there is no resistance and a situation of perfect slip is present. When $S \to \infty$, there is infinite resistance at the bottom and therefore no slip. In reality the value of S

will be somewhere between these theoretical cases and can, for instance, be related with to bed roughness (Hulscher, 1996; Németh, 2003).

The boundary conditions at the free surface state that there is no friction and no flow through the free surface:

$$\left.\frac{\partial u}{\partial z}=0\right|_{z=H+\zeta(x,t)}, \tag{5.5}$$

and

$$w=\left.\frac{\partial \zeta}{\partial t}+u\frac{\partial \zeta}{\partial x}\right|_{z=H+\zeta(x,t)}. \tag{5.6}$$

Finally, a second boundary condition at the seabed,

$$\left.w-u\frac{\partial h}{\partial x}=0\right|_{z=h(x)}, \tag{5.7}$$

states that there is also no flow through the bed.

5.1.2 Sediment transport

The water flow induces a volumetric bed shear stress, τ (m^2/s^2), which can be calculated directly from the flow:

$$\tau=A_v\left.\frac{\partial u}{\partial z}\right|_{z=h(x)}. \tag{5.8}$$

The bed shear stress can move grains and therefore sediment can be transported. To calculate this sediment transport, a general bed load formula is used (For an explanation see Komarova and Hulscher, 2000):

$$q=\alpha\sqrt{|\tau|}\left[\tau-\lambda|\tau|\frac{\partial h}{\partial x}\right]. \tag{5.9}$$

This equation only describes bed load transport, q (m^2/s), which is assumed to be dominant in offshore tidal regimes. λ (-) is a parameter for the bed slope mechanism and α (s^2/m) is a bed load transport proportionality parameter. α is set at a value of about 0.3 s^2/m and incorporates the porosity of the bed. The sediment transport model is coupled with the flow model with the sediment balance:

$$\frac{\partial h}{\partial t}=-\frac{\partial q}{\partial x}. \tag{5.10}$$

This equation does not involve the porosity as that is already included in the definition of q (equation (5.9)). The sediment continuity equation states the conservation of mass for the sediment.

5.1.3 Stability approach

For this research, the flat bed is initially perturbed with a small disturbance, a sinusoidal wave with a certain wavelength and small amplitude. The disturbance may develop into a sandwave, which means that the bed is unstable. For different wavelengths, different simulations are done, to investigate the initial behaviour of the sandwave. The sandwave which grows fastest in the linear regime is assumed to dominate the bed evolution. The wavelength of this sandwave is called the fastest growing mode.

5.2 Sediment transport equation

The code included a rewritten version (equation (5.9)) of the Meyer-Peter and Müller sediment transport equation (Komarova and Hulscher, 2000). This equation is only indirectly depending on the grain size. For the aim of this research, modelling the relevant processes for heterogeneous sediment, a transport equation that includes a value for the grain size, is necessary. Van der Scheer et al. (2002) gives an overview of transport equations that are suitable for heterogeneous sediment modelling. One of these equations is the original Meyer-Peter and Müller equation. This is an equation for bed-load transport that is directly grain size dependent. It has a clear physical structure and is used in earlier research on tidal sandwaves (Van der Meer et al., 2005). For comparison reasons and for a good understanding this equation will be used here.

5.2.1 Meyer-Peter and Müller for homogeneous sediment

The Meyer-Peter and Müller equation (as described in Van Rijn, 1993), reads:

$$q = 8(s-1)^{0.5} g^{0.5} D_m^{\ 1.5} (\mu\theta - \theta_{cr})^{1.5}, \tag{5.11}$$

with:

$$\theta = \frac{\tau}{(s-1)gD_m}, \tag{5.12}$$

$$s = \frac{\rho_s}{\rho}, \tag{5.13}$$

q	=	bed-load transport rate (m^2/s)
g	=	acceleration due to gravity ($9.81 m/s^2$)
D_m	=	grain diameter (m)
θ	=	dimensionless Shields parameter (-)
θ_{cr}	=	critical dimensionless Shields parameter (-)
τ	=	volumetric bed shear stress (m^2/s^2)
s	=	specific density (-)
ρ	=	fluid density ($1.0*10^3$ kg/m^3)
ρ_s	=	sediment density ($2.65*10^3$ kg/m^3)
μ	=	bed form factor (-)

Note that the porosity is not incorporated within this transport rate and therefore should be taken into account in the sediment continuity equation.

The bed form factor μ accounts for the presence of other bedforms superimposed on the sandwaves. Initially the sandwaves will be considered as separate bedforms, not influenced by other bedforms. In this case μ equals 1.

For comparison reasons, an equation is used for the critical Shields parameter that is also used in earlier research about sandwaves (Van der Meer et al., 2005). It can be calculated with the empirical expression, according to Soulsby (1997) and references herein:

$$\theta_{cr,m} = \frac{0.24}{D*_m} + 0.055[1 - \exp(-0.02 D*_m)] , \tag{5.14}$$

$$D*_m = \left[\frac{g(s-1)}{\nu^2} \right]^{1/3} D_m , \tag{5.15}$$

with:

$\theta_{cr,m}$	=	critical Shields parameter based on the mean grain size D_m (-)
$D*_m$	=	dimensionless mean grain size (-)
ν	=	kinematic viscosity of water (1.36*10^{-6} m^2/s)

For the D_m (m) in equation (5.11) and (5.15), a value that represents the grain size, or diameter, of the sediment must be used. The median grain size (D_{50}) can be used, or the mean grain size. Since Meyer-Peter and Müller (1948) describes their D_m as the mean grain size and states that this mean grain size is approximately equal to D_{50}, the mean grain size is also used here:

$$D_m = \sum_i^N F_i D_i , \tag{5.16}$$

with:

F_i	=	fraction of size class i in the bed material (-)
D_i	=	grain size of size class i (m)
N	=	number of classes (-)

Note that this is the same equation as equation (3.4).

The part ($\mu\theta$ - θ_{cr}) in equation (5.11) states that a grain can only be moved when the (dimensionless) shear stress that acts on that grain exceeds the critical (dimensionless) shear stress of that grain. The latter is the minimal shear stress that is required to move a grain. When this critical shear stress is left out of consideration, the $D_m^{-1.5}$ in the θ will completely counteract the $D_m^{1.5}$ and the equation becomes grain size independent. The critical shear stress, however, accounts for the effects that stop grains from getting in motion; for instance gravity or the influence of surrounding (same sized) particles. When this critical shear stress will be left out of equation (5.8), the total sediment transport may be over predicted.

Van Rijn (1993) states that the Meyer-Peter and Müller equation, although weakly, is dependent on the grain size. Van der Meer et al. (2005) found that the grain size in this equation influenced the sandwave height in simulations.

5.2.2 Meyer-Peter and Müller extended for the case of sandwaves

In the case of sandwaves, the bed shear stress is caused by the tidal wave. That means that the shear stress can be either positive or negative. Therefore the shear stress and accordingly the sediment transport have a direction; sand can be moved from one side to another, or the opposite way. The magnitude of the shear stress acting on the grains, is independent of the direction of this shear stress. When using equation (5.11), the part ($\mu\theta$ -θ_{cr}) causes a change in the amount of sediment transport, if the direction of the flow (and therefore the direction of the (dimensionless) shear stress) changed. Therefore the absolute value of the dimensionless shear stress is taken. To give direction to the sediment transport, a factor $\tau / |\tau|$ is included.

Equation (5.11) also lacks the influence of the bottom slope of sandwaves. To overcome this problem an extra slope factor is included. This factor accounts for the effect that the grains move easier from the crest to the trough than the other way around. The total extra factor B (-) becomes:

$$B = \frac{\tau}{|\tau|} - \frac{dh/dx}{\tan\phi_s}, \tag{5.17}$$

with:

h = bed elevation (m)

ϕ_s = correction factor for angle of repose of sand

(tan ϕ_s = 0.3 following Komarova and Hulscher, 2000).

After these extensions for the case of sandwaves, the transport equation reads:

$$q = 8(s-1)^{0.5} g^{0.5} D_m^{\ 1.5} (\mu|\theta| - \theta_{cr})^{1.5} B\,. \tag{5.18}$$

5.2.3 Meyer-Peter and Müller for heterogeneous sediment

To model heterogeneous sediment, the bed material will be divided in a number of size fractions and the sediment transport equation will be applied for each size fraction.

A correction factor is used to account for the hiding-exposure effect (Van Rijn, 1993). This effect is the result of the interaction between different grain sizes. In the presence of finer grains, coarser grains protrude more into the flow and are therefore more exposed to the drag force. That means that they are easier transported and that smaller critical shear stresses are needed to bring these coarser grains in motion, than in the case of uniform sediment of this grain size. Conversely, finer grains can hide behind and between coarse grains. They experience a smaller drag force and are less easier transported than in corresponding uniform sediment and therefore larger critical shear stresses are needed to bring them into motion. Together this is called the hiding-exposure effect (Parker, 2005; Seminara, 1995). This effect reduces the difference in critical (dimensionless) shear stress required to move different grain sizes and therefore this critical (dimensionless) shear stress is often corrected using a hiding-exposure factor, ξ_i (-):

$$\theta_{cr,i,corrected} = \xi_i \theta_{cr,m}, \tag{5.19}$$

with

$\theta_{cr,i,corrected}$ = corrected critical Shields parameter for grain size i (-)

$\theta_{cr,,m}$ = critical Shields parameter based on the mean grain size D_m (-)

(For more information about this standard correction see Kleinhans, 2002.)

A hiding exposure factor that is commonly used in combination with the Meyer-Peter & Müller transport equation is proposed by Egiazaroff (1965):

$$\xi_i = \left[\frac{\log(19)}{\log(19 D_i / D_m)} \right]^2 . \tag{5.20}$$

It corrects the critical dimensionless Shields parameter that is based on the mean grain size D_m (Van Rijn, 1993). This hiding-exposure factor is semi-theoretically determined. In the theoretical case of homogeneous sediment, there is only one grain size class and D_i has the same value as D_m. Then the correction factor becomes 1. The (dimensionless) critical shear stress, multiplied by 1, remains the same. To provide a good understanding, this relative simple hiding-exposure factor will also be used here.

According to Van Rijn (1993), the total transport rate for all fractions using the Meyer-Peter and Müller equation, becomes:

$$q = 8(s-1)^{0.5} g^{0.5} \sum_{i=1}^{N} F_i D_i^{1.5} (\mu |\theta_i| - \xi_i \theta_{cr,m})^{1.5} B , \tag{5.21}$$

in which θ_i is the critical Shields parameter for grain size class i:

$$\theta_i = \frac{\tau}{(s-1) g D_i} . \tag{5.22}$$

The equation to calculate the transport rate q_i (m^2/s) for each size class i, as it is implemented in the code, becomes:

$$q_i = \begin{cases} 0 & if \quad \mu |\theta_i| - \xi_i \theta_{cr,m} < 0 \\ 8(s-1)^{0.5} g^{0.5} F_i D_i^{1.5} (\mu |\theta_i| - \xi_i \theta_{cr,m})^{1.5} B & if \quad \mu |\theta_i| - \xi_i \theta_{cr,m} > 0 \end{cases} . \tag{5.23}$$

5.3 Sediment continuity equation

For heterogeneous sediment a more complicated sediment continuity equation is required than the sediment balance (equation (5.10)) for homogeneous sediment. In the case of heterogeneous sediment, besides divergences in the total sediment transport rate, also divergences in the transport rate of size fractions exist. Furthermore the bed composition can vary, that means that the (percentage of the) fractions in the bed will not remain the same on each place. Therefore a different type of sediment continuity model is needed. Different models can be used. (For an overview see Blom, 2003). From these models, the Hirano active layer model is one of the most well-known (Blom, 2003 and references herein).

In this active layer model, the bed is divided in an active layer and a non-moving substrate, figure 5.3. Both layers have a specific composition of grain size fractions.

Only the active (surface) layer contains material available for transport. That means that the active layer thickness can be defined as the thickness of the bed at which, on a certain moment, the grains experience the drag of the flow. Therefore this active layer thickness is usually in the order of a few grain sizes. (For more information see Blom, 2003.) In this case the thickness is assumed to be constant.

The substrate does not interact with the flow directly. The sediment from the substrate can only be entrained into the flow after being entrained into the active layer. Because the substrate is large in comparison to the active layer, it is assumed that sediment which becomes part of the substrate after sedimentation, is immediately mixed with the sediment of the substrate, which results in a constant grain size distribution in the substrate. In case of net erosion, the interface between the active layer and the substrate will lower, which induces a sediment flux (with the same grain size distribution as in the substrate) from the substrate to the active layer. (See also figure 5.4.) In case of net sedimentation, the opposite happens. A sediment flux occurs from the active layer to the substrate through a rise in the interface between the active layer and the substrate. Although this sediment flux will have the grain size distribution of the active layer, the complete grain size distribution of the substrate will not change. Therefore only the grain size distribution in the active layer can change.

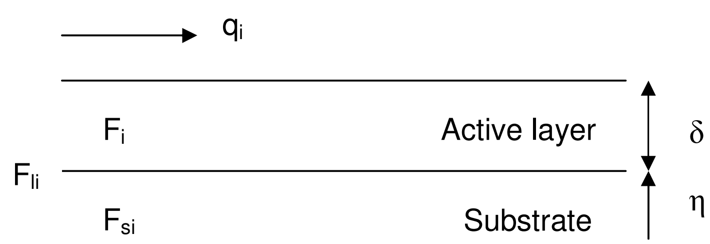

Figure 5.3: The active layer model

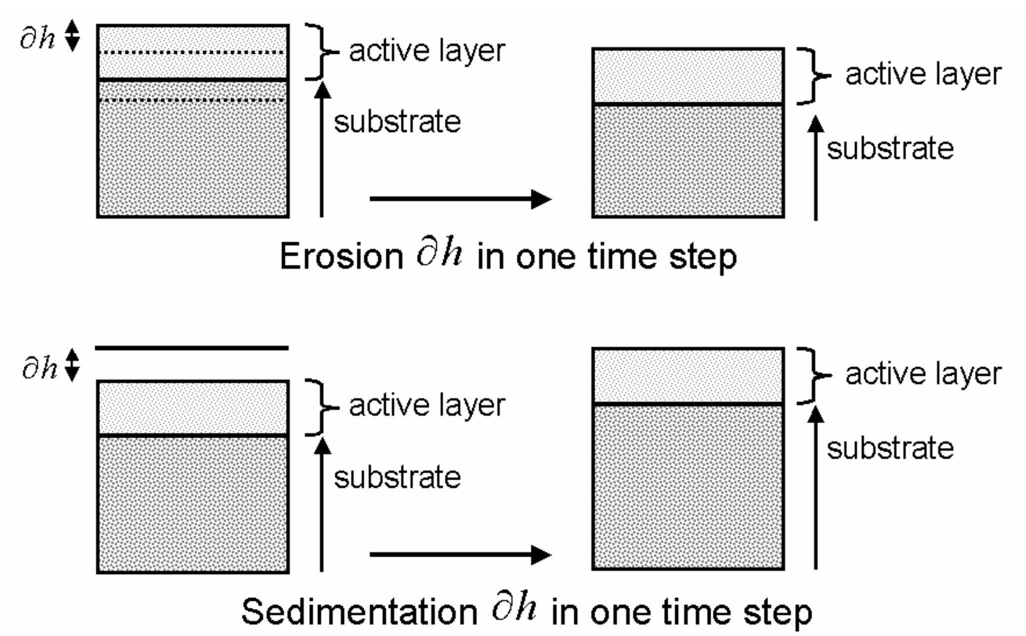

Figure 5.4: The active layer model

The changes in the active layer can be calculated with the equation:

$$c_b \delta \frac{\partial F_i}{\partial t} + c_b F_{Ii} \frac{\partial \eta}{\partial t} = -\frac{\partial q_i}{\partial x}, \tag{5.24}$$

where

$$F_{Ii} = \begin{cases} F_i & \text{if } \frac{\partial \eta}{\partial t} > 0 \\ F_{si} & \text{if } \frac{\partial \eta}{\partial t} < 0 \end{cases},$$

in which:

q_i	=	bed-load transport of size class i (m^2/s)
F_i	=	volume fraction of size class i in the active layer (-)
F_{Ii}	=	volume fraction of size class i at the interface between the active layer and the substrate (-)
F_{si}	=	volume fraction of size class i in the substrate (-)
c_b	=	sediment concentration in the bed (1-porosity) (0.6)(-)
δ	=	thickness of the active layer (m)
η	=	elevation of the interface (m)

Note that the elevation η is the elevation caused by the total transport rate.
Because the fractions must satisfy the constraint

$$\sum_{i=1}^{N} F_i = 1, \tag{5.25}$$

the total equation can be solved first:

$$c_b \frac{\partial \eta}{\partial t} = -\frac{\partial \sum_i q_i}{\partial x}. \tag{5.26}$$

From this it is known whether there is erosion or sedimentation, and equation (5.24) can be solved. With this equation (5.24) not only the change of bottom elevation can be calculated, but also the local change of the sediment fractions.
Finally the resulting height of the bed can be given through:

$$h = \eta + \delta. \tag{5.27}$$

Appendix 5 gives an explanation of how these equations must be solved in the code.

6. Results

In order to find out whether the new model, as described in the previous chapter, can make grain size sorting visible, the additional equations for heterogeneous sediment are implemented in a numerical code, developed by Van den Berg (Van den Berg and Van Damme, 2005). First the results of a reference simulation for two grain size fractions are given. To provide insight in the influence of heterogeneous sediment, the results of the reference simulation are also compared with the results of a corresponding simulation for homogeneous sediment. For a better understanding of the influence of different factors, other simulations have been carried out and their results are compared with the results of the reference simulation.

6.1 The reference simulation

6.1.1 The reference simulation for heterogeneous sediment

A bimodal mixture with more or less realistic values for the grain sizes is sufficient, to model grain size sorting over sandwaves. Working with only two fractions, provides a good insight in the behaviour of the fractions.

For a rough indication of realistic grain sizes for sandwaves, the received data from TNO for the offshore sandwave field are used. The different values for D_{50} from these data are averaged. This gives an averaged value of 285 μm. The same is done for the values for D_{10} and D_{90}, this gives averaged values of 205 μm and 397 μm respectively.

For the first simulation, a coarse fraction is used with a grain size of 400 μm and a fine fraction with a grain size of 200 μm. This gives a mean grain size of 300 μm. It is assumed that in the initial situation, the bed is perfectly mixed, and the substrate has the same distribution as the active layer. Therefore, both compositions start with the same distribution. For the reference simulation 50% is used for each fraction. As an initial profile, the bed is perturbed with a sinusoidal wave, with an amplitude of 0.3 m. The active layer thickness is set at 2 mm, which is in the order of a few grains.

In order to find the fastest growing wavelength, the initial evolution of a sandwave is simulated for different wavelengths with intervals of 50 meter. For this reference case a sandwave length of 650 meter is found. Note that this is only an approximation of the fastest growing mode. For this wavelength the intermediate term behaviour is simulated.

It turns out that the evolution of the fractions in the active layer can be simulated for about the first ten years of the development of a sandwave. After that, the calculation of the fractions becomes unstable, although the sandwave still develops further.

Figure 6.1a shows the development of the fractional distribution in the active layer, over the length of one sandwave. The corresponding sandwave is plotted in figure 6.1b.

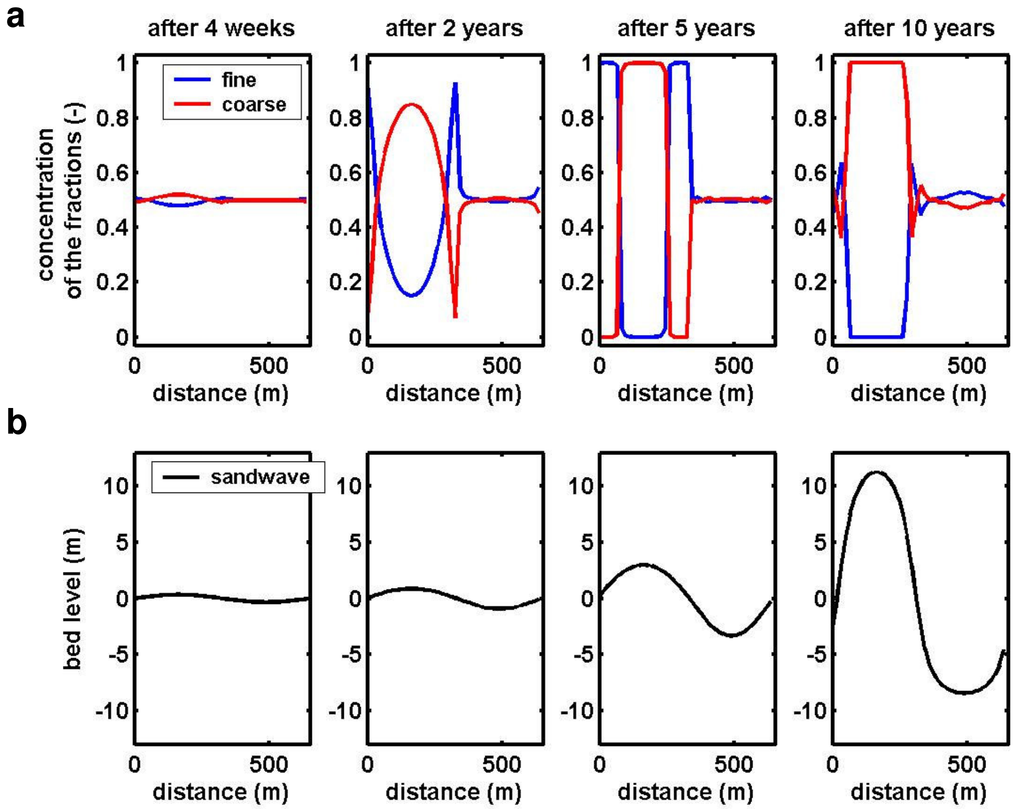

Figure 6.1: Coarse and fine sediment concentration in the active layer along a sandwave profile at different times: (a) evolution of fractions in the active layer; (b) development of sandwave morphology.

The fractions show opposite behaviour around the horizontal line F = 0.5 (=50%), which results directly from the fact that the total amount of the two fractions in the active layer always equals 100%. Also the concentration of a fraction in the active layer remains always between 0 and 1, which is realistic, as there can not be less than 0% or more than 100% of a fraction in nature.

Figure 6.1 show the concentration of the fractions not everywhere equals 0.5. When one fraction gets a higher concentration than the other, it means that in the active layer on that place more grains of one fraction are present. Accordingly, the grains are sorted over the sandwave.

In figure 6.2, 6.3 and 6.4, the development of the fractional composition in the active layer is plotted for respectively a point in the middle of the sandwave slope, a point in the middle of the sandwave crest and a point in the middle of the sandwave trough for the first ten years of the sandwave evolution.

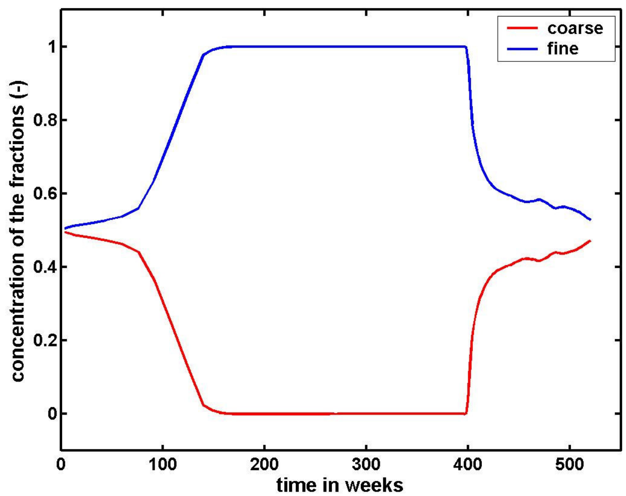

Figure 6.2: Development of grain size composition on the sandwave slope, at x =325 meter.

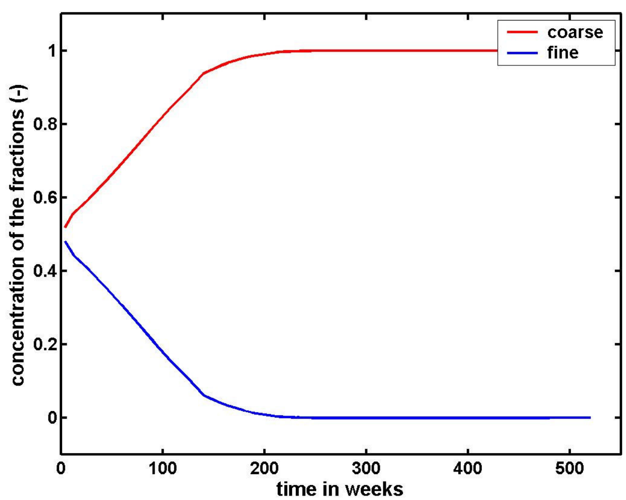

Figure 6.3: Development of grain size composition on the sandwave crest, at x =162.5 meter.

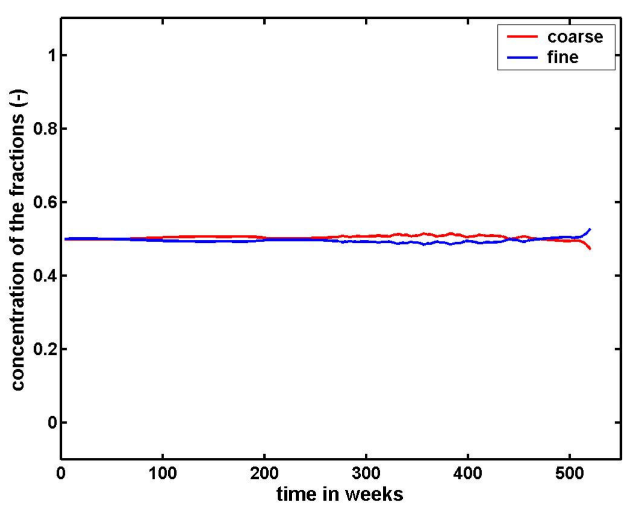

Figure 6.4: Development of grain size composition on the sandwave trough, at x = 487.5.

After about 4 years, the concentration of the coarse fraction in the active layer becomes 1 at the sandwave crest whereas the concentration of the fine fraction becomes 0. In that case only coarser grains are present in the active layer on the crest.

On the slope the opposite happens. After about 3 years a concentration of 1 for the fine fraction in the active layer is reached. However, after about 10 years the fine fraction is disappeared from the slope. Figure 6.2 shows a sudden regression of the fine fraction after 8 years. This is due to the fact that the slope about this time slightly moved (see figure 6.5b) and therefore the point for which the fractions are plotted in figure 6.2 is no longer the middle point of the slope. In figure 6.1a a sharp peak can be observed on the slope during the first years, but after some time this peak decreases.

In the troughs the concentration of the fractions in the active layer remain both around 0.5, although figure 6.1 shows that after 10 years the fine fraction has slightly increased here. Figure 6.4 shows that this increasing behaviour only begins after approximately 10 years.

The sandwave grows relatively fast during the first ten years. Within this time the crest grows up to almost 12 meters. After that time, the sandwave still develops, but now also its shape changes. This is shown in figure 6.5.

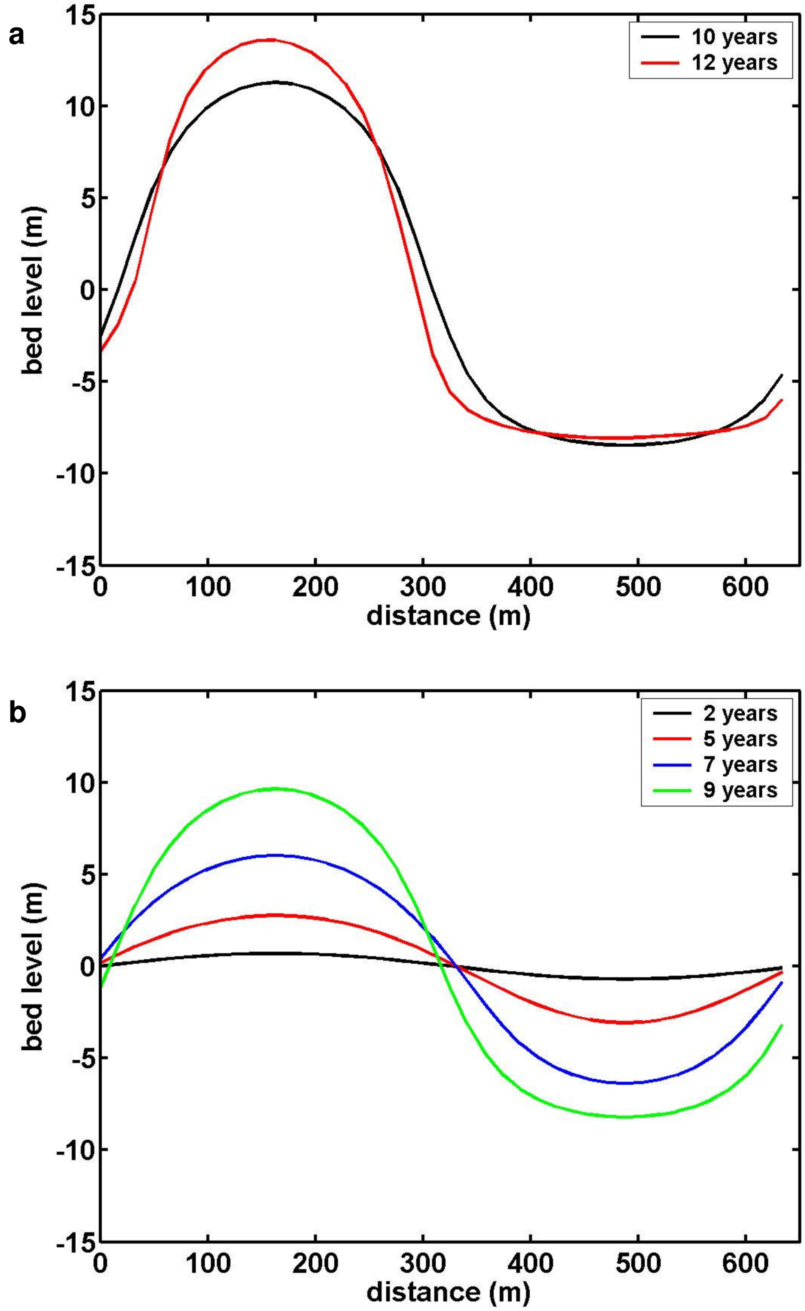

Figure 6.5b: Shape of sandwave: (a) after 10 and 12 years; (b) after 2, 5, 7 and 9 years.

6.1.2 The simulation for homogeneous sediment

To get insight in the influence of the heterogeneous sediment on the sandwave characteristics, the results of the reference simulation are compared with the results of a simulation for homogeneous sediment. For the homogeneous case one fraction is simulated with a percentage of 100%. For this fraction a grain size of 300 μm is used, as this is the mean grain size of the two fractions from the reference simulation.

The concentration of these fractions remains 1 everywhere, because sorting is impossible now.

Again the initial evolutions of a sandwave are simulated for different values for the sandwave length with intervals of 50 meter. It turns out that again the sandwave with length 650 meter grows fastest. This sandwave develops the same as the one with heterogeneous sediment. Therefore also the sandwave height is the same on the same time in both cases. Apparently the heterogeneous sediment seems to have no influence on the sandwave dimensions.

6.2 Simulations with different settings

6.2.1 Smaller differences between the grain sizes

To investigate the influence of grain sizes, first the difference between the grain sizes of the fractions are change. Now, a simulation is done with grain sizes 250 μm and 350 μm instead of grain sizes of 200 μm and 400 μm. This still gives the same mean grain size of 300 μm. The other parameters remain unchanged. The results of this simulation can be seen in figure 6.6. For a better insight now only the development of the fine fraction is shown. Figure 6.6a shows the results of the reference simulation, for comparison. Figure 6.6b shows the results for the new settings and figure 6.6c the sandwave development for this simulation.

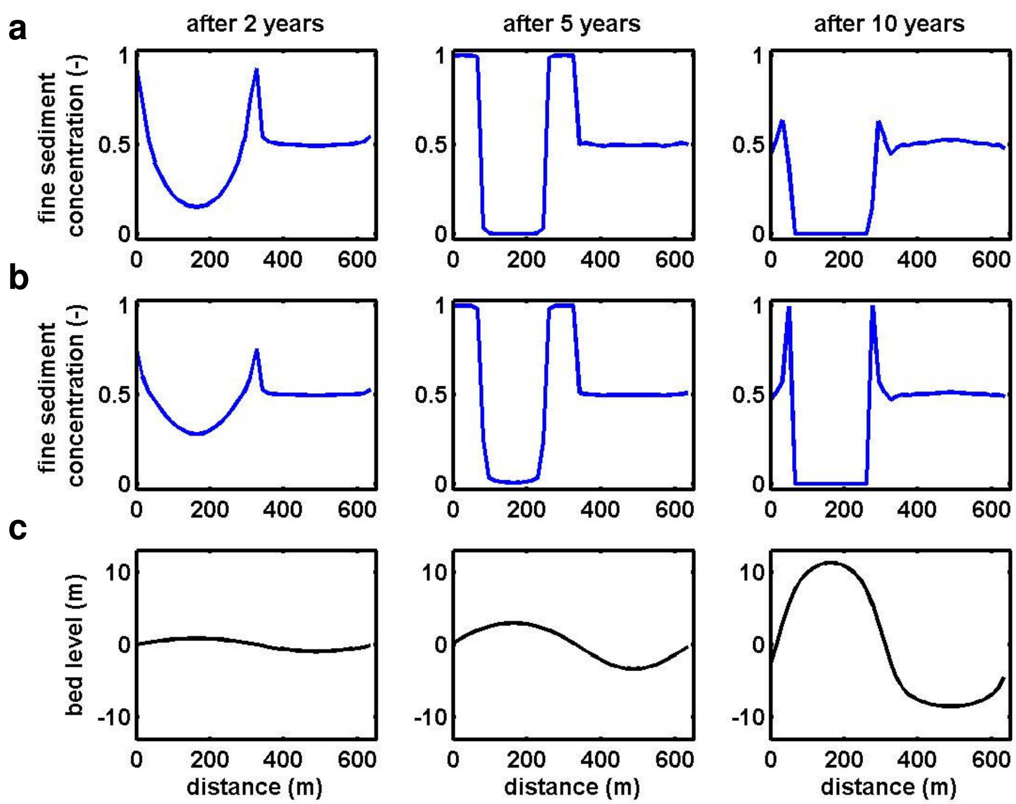

Figure 6.6: Fine sediment concentration in the active layer along a sandwave profile at different times: (a) reference simulation; (b) simulation with grain sizes 250 μm and 350 μm; (c) development of sandwave morphology.

For the new simulation, the same effects are visible, although slightly less pronounced. After 2 years the behaviour of the fine fraction for the new case is somewhat less developed than in the reference run and after 10 years the peaks are less reduced. The slower development of the grain size sorting is the direct result from the smaller difference in grain size.

The fastest growing mode for this new case is still 650 meter (determined on the same way). The simulation for the accompanying homogeneous sediment case is the same as for the reference simulation. For both cases the mean grain size is 300 μm.

6.2.2 Larger grain sizes

Now the effect of larger values is investigated. Again the values of other parameters remain the same. Two simulations were done, one with grain sizes 400 μm and 600 μm (figure 6.7) and one with 900 μm and 1100 μm (figure 6.8). Note that, although the absolute differences between these grain sizes are still the same (200 μm), the relative differences become smaller.

Again the fastest growing wavelength is investigated. It turns out that for grain sizes 400 μm and 600 μm, the wavelength remains unchanged. For grain sizes 900 μm and 1100 μm however, the fastest growing wavelength becomes 600 meter (for intervals of 50 meter). The simulation with these grain sizes is therefore done with this smaller wavelength. To see the difference between in the development of both sandwaves (one with a length of 600 meter and one with a wavelength of 650 meter), figure 6.9 shows these sandwaves after a development of 10 years. The sandwave with length 600 meter then is a bit smaller than the other sandwave.

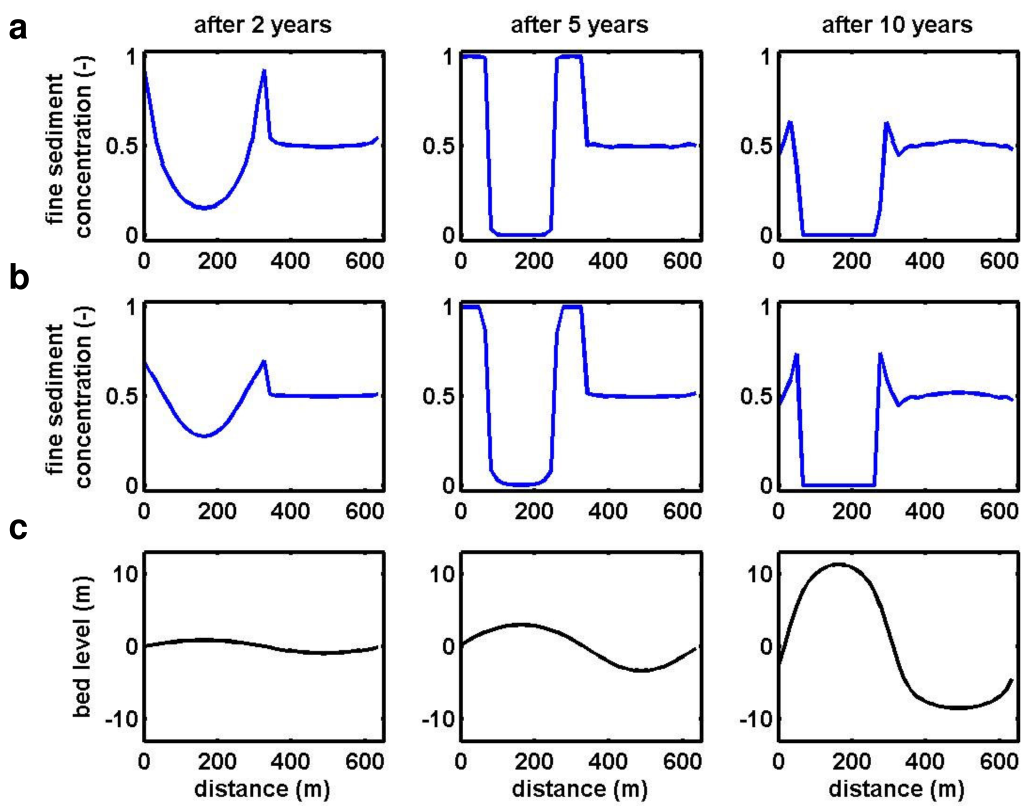

Figure 6.7: Fine sediment concentration in the active layer along a sandwave profile at different times: (a) reference simulation; (b) simulation with grain sizes 400 μm and 600 μm; (c) development of sandwave morphology.

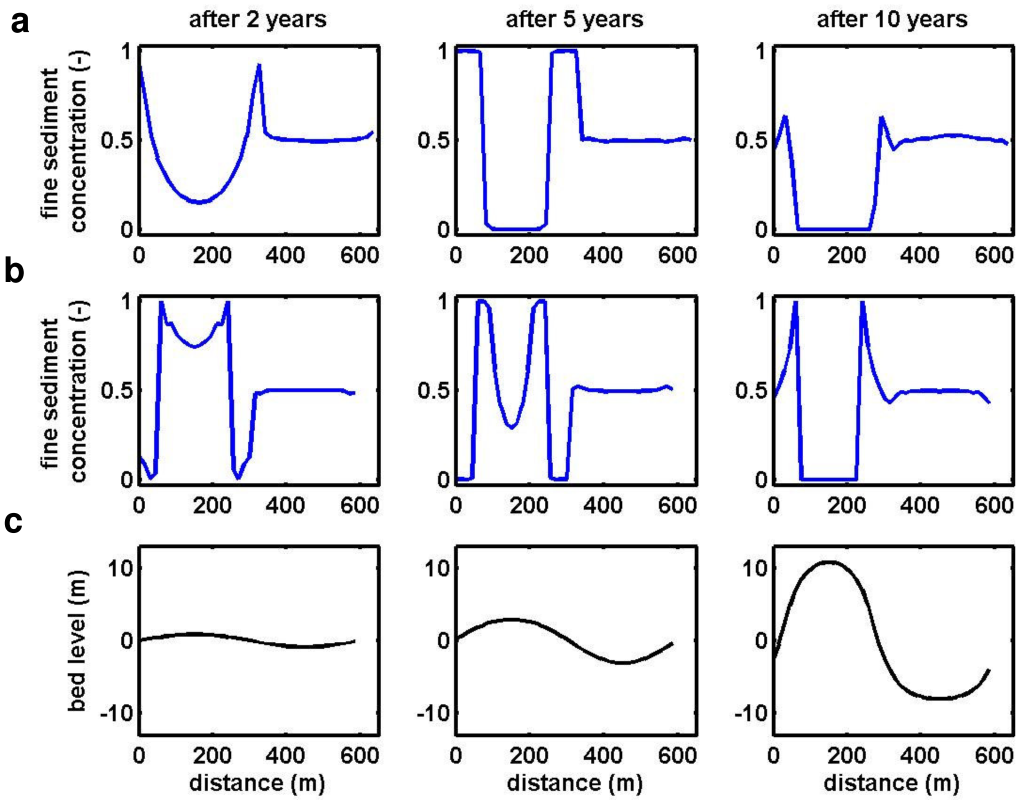

Figure 6.8: Fine sediment concentration in the active layer along a sandwave profile at different times: (a) reference simulation; (b) simulation with grain sizes 900 μm and 1100 μm; (c) development of sandwave morphology.

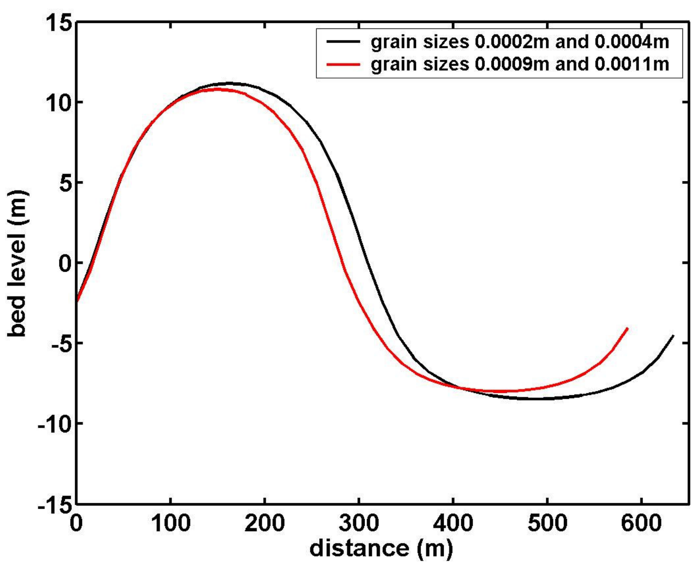

Figure 6.9: Development of a sandwave with grain sizes 200 and 400 μm and sandwave with grain sizes 900 and 1100 μm after 10 years.

Figure 6.7 shows no difference between the reference simulation and the simulation with grain size 40 and 600 µm, except for the plot of two years, where the evolution of the fine fraction seems less pronounced than in the reference case.

The simulation for grain sizes of 900 and 1100 µm, however, seem to be very different from the reference simulation in the first few years. Instead of the coarse fraction, now the fine fraction accumulates at the crest. In the middle of the crest however, the fine grains are disappearing. After ten years, the concentration of the fine fraction in the active layer on the crest is again 0, as in the reference simulation.

This might be caused by the unaltered active layer thickness. The active layer thickness is defined as the thickness at which the grains at a certain moment are directly influenced by the flow. It is therefore in the order of a few grains. When the considered grains are much larger, the active layer thickness should become larger as well. Therefore a new simulation is done for the grain sizes 900 and 1100 µm, with an active layer thickness of 5.5 mm (five times the coarser grain size, because 2 mm was five times the coarser grain of 400 µm). The results of this new simulation are shown in figure 6.10.

It turns out that the behaviour of the fine fraction is the same as in the case of an active layer of 2 mm, but less pronounced. After 10 years the distribution of the fractions in the active layer is almost completely the same as in the reference case.

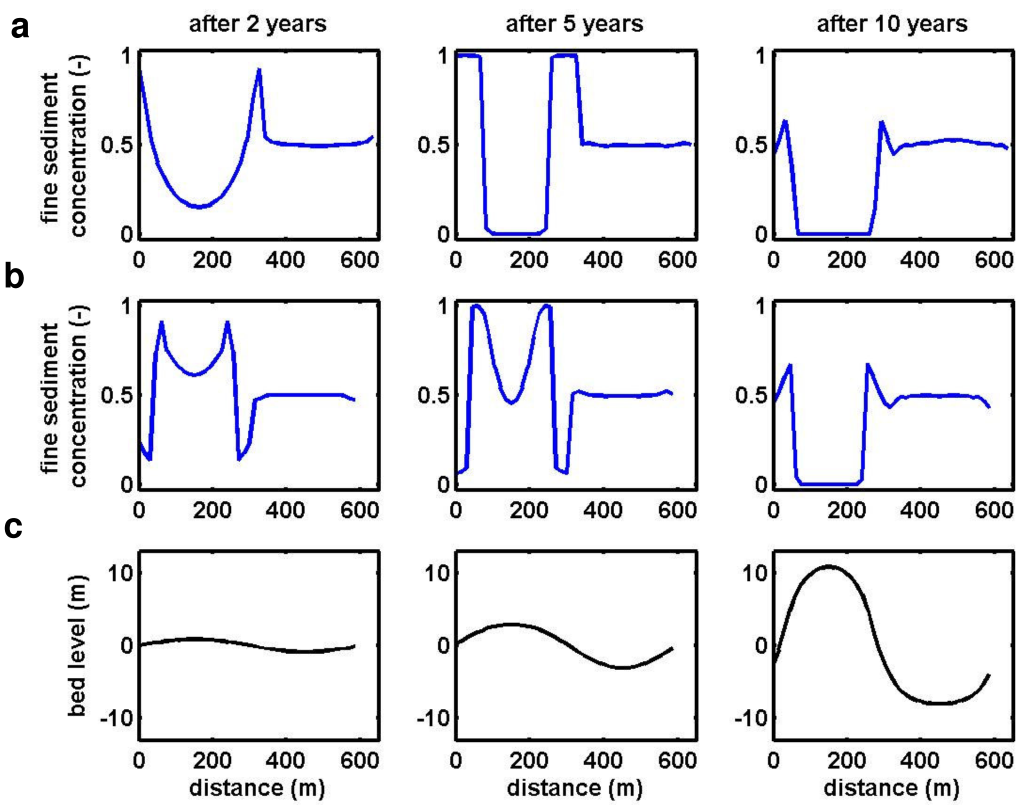

Figure 6.10: Fine sediment concentration in the adapted active layer, along a sandwave profile at different times: (a) reference simulation; (b) simulation with grain sizes 900 µm and 1100 µm and an active layer thickness of 5.5mm; (c) development of sandwave morphology.

6.2.3 A simulation without hiding-exposure

To investigate the influence of the hiding-exposure factor, a simulation is done without the correction factor, ξ_i. The other parameters are the same as in the reference simulation. The results are shown in figure 6.11. Again the coarser fraction accumulates at the crest and the finer fraction at to the slope. The evolution of the fractions seems to be more extreme, compared with the reference simulation. Maybe due to this stronger development, there is a stronger increase of the fine fraction in the trough after 10 years. The wavelength for this case turns out to be the same as for the reference simulation.

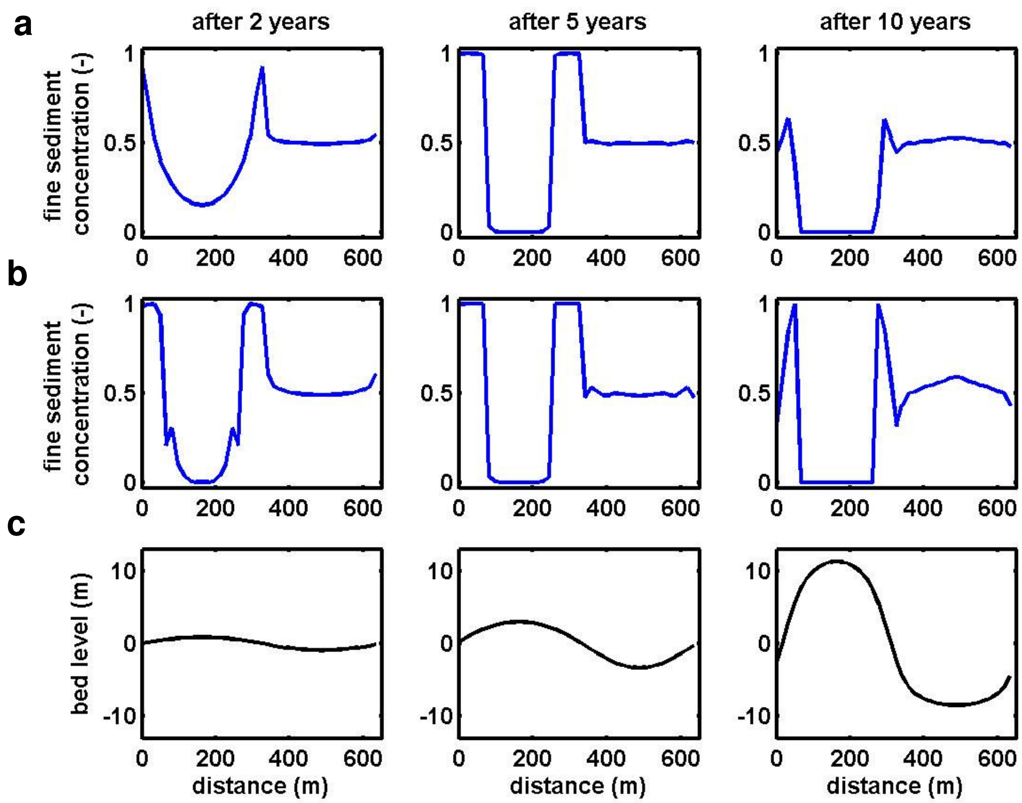

Figure 6.11: The development of the fractions in the active layer, without hiding-exposure effect: (a) reference simulation; (b) simulation without hiding-exposure factor; (c) development of sandwave morphology.

6.2.4 Different percentages for the fractions

For all the previous described simulations, the initial percentage of the fractions in the active layer are equal (both 50%). To see the effect of this initial distribution, another simulation is done with different initial values for the percentage of the fractions in the active layer; 70% fine sediment and 30% coarse sediment on each location in the active layer. Because the sediment in the substrate is assumed to have the same grain size distribution as the initial distribution of the active layer, it was also set on 70% fine and 30% coarse sediment. The other parameters are not changed, this means that the grain sizes are the same as in the reference simulation and hiding-exposure is taken into account.

Figure 6.12 shows no large difference between the behaviour of the fractions in the active layer, compared with the reference simulation. The only real difference is in the sandwave trough, because the fractions initial have another concentration and remains during the 10 years almost the same. Also for the wavelength the same value of 650 meter is found.

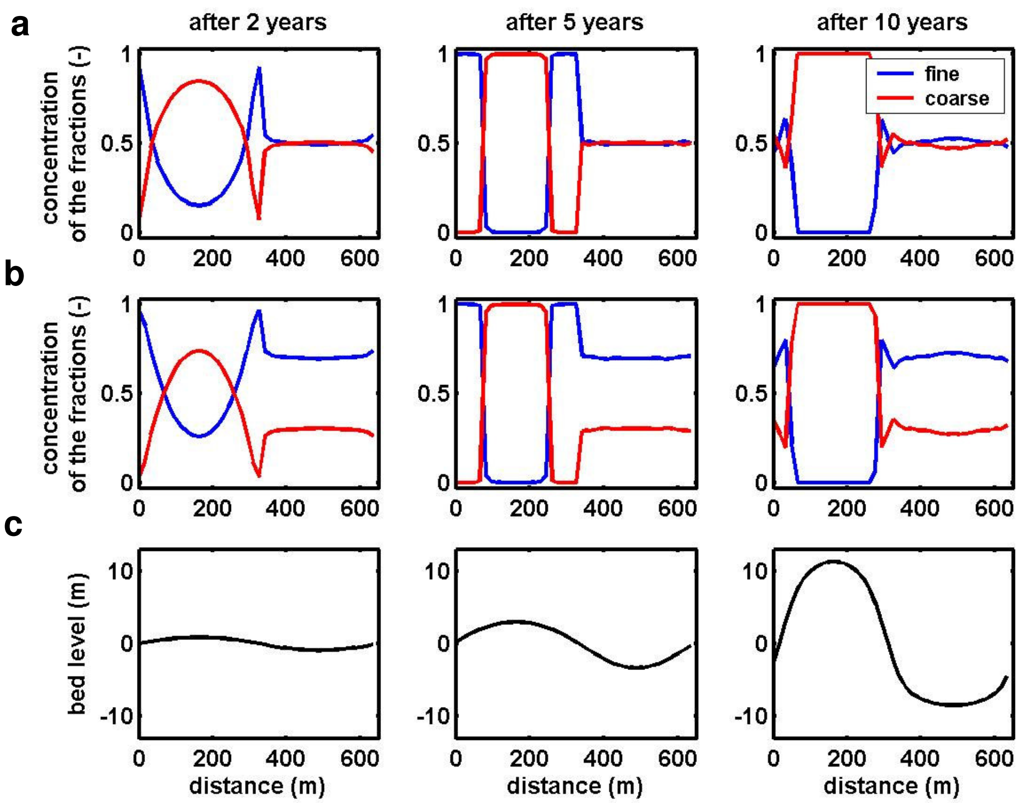

Figure 6.12: Coarse and fine sediment concentration in the active layer along a sandwave profile at different times: (a) reference simulation; (b) simulation with initial concentrations of 0.3 fine and 0.7 coarse sediment; (c) development of sandwave morphology.

6.2.5 Three classes

It is also possible to model grain size sorting with more than only two classes. Figure 6.13 shows the results of a simulation with three fractions, all with $33\frac{1}{3}$% and grain sizes 200, 300 and 400 µm. This again gives a mean grain size of 300 µm.

The coarse (400 µm) and the fine (200 µm) fraction in the active layer acts approximately the same as in the case of only two fractions. Fine grains leave the crest and accumulate at the slope. Coarser grains on the other hand leave the slope and accumulate at the crest. The medium fraction (300 µm) remains in the beginning near the $33\frac{1}{3}$%. The medium grain size is leaving the crest, and therefore behaves the same as the fine fraction, although less pronounced. On the slope however, after 2 and 5 years it behaves more like the coarse fraction, because it disappears here. After 10 years it is almost the same as the fine fraction.

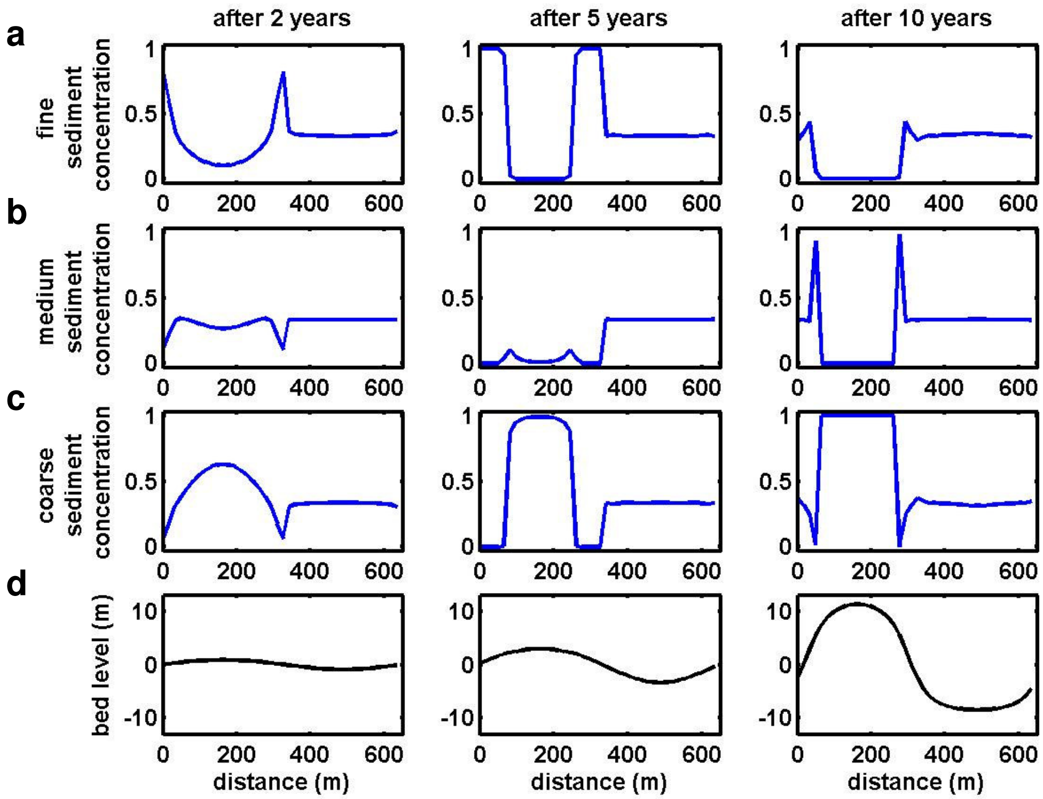

Figure 6.13: Sediment concentration of the different fractions in the active layer along a sandwave profile at different times: (a) concentration of the fine sediment in the active layer; (b) concentration of the medium sediment in the active layer; (c) concentration of the fine sediment in the active layer; (d) development of sandwave morphology.

7. Discussion

In this chapter the results of the model are discussed. Therefore first the influence of the chosen model is considered. After that, the model results are discussed in relation to the field observations.

7.1 Discussion of the used equations

7.1.1 The active layer

Some of the behaviour of the fractions can be explained by the characteristics of the used active layer model. For convenience the equation (5.24) is repeated here:

$$c_b\delta\frac{\partial F_i}{\partial t}+c_bF_{Ii}\frac{\partial \eta}{\partial t}=-\frac{\partial q_i}{\partial x}, \tag{5.24}$$

where

$$F_{Ii}=\begin{cases}F_i & \text{if } \frac{\partial\eta}{\partial t}>0\\ F_{si} & \text{if } \frac{\partial\eta}{\partial t}<0\end{cases}.$$

When $\frac{\partial\eta}{\partial t}$ = 0, the term $c_bF_{Ii}\frac{\partial\eta}{\partial t}$ = 0 and both parts are equal. Therefore

$$\lim_{\frac{\partial\eta}{\partial t}\uparrow 0}\left(c_bF_{Ii}\frac{\partial\eta}{\partial t}\right)=\lim_{\frac{\partial\eta}{\partial t}\downarrow 0}\left(c_bF_{Ii}\frac{\partial\eta}{\partial t}\right)$$

and the active layer model is continuous in this point. The distribution of the fractions in the active layer is calculated over the profile of the sandwave. When looking at the derivate in horizontal direction of equation (5.12), the term $c_bF_{Ii}\frac{\partial\eta}{\partial t}$ becomes:

$$\frac{\partial}{\partial x}\left(c_bF_{Ii}\frac{\partial\eta}{\partial t}\right)=c_b\left(\frac{\partial F_{Ii}}{\partial x}\frac{\partial\eta}{\partial t}+F_{Ii}\frac{\partial^2\eta}{\partial t\partial x}\right).$$

The term $F_{Ii}\frac{\partial^2\eta}{\partial t\partial x}$ not necessarily goes to zero with $\frac{\partial\eta}{\partial t}$. Therefore

$$\lim_{\frac{\partial\eta}{\partial t}\uparrow 0}\frac{\partial}{\partial x}\left(c_bF_{Ii}\frac{\partial\eta}{\partial t}\right)\neq\lim_{\frac{\partial\eta}{\partial t}\downarrow 0}\frac{\partial}{\partial x}\left(c_bF_{Ii}\frac{\partial\eta}{\partial t}\right)$$

The active layer model is non differentiable at $\frac{\partial\eta}{\partial t}$ = 0.

From figure 6.5b (or 6.1) it can be observed that h (= $\eta+\delta$) remains zero on the middle of the sandwave and therefore $\frac{\partial\eta}{\partial t}$ remains also 0 on this point. When looking at the development of the fractions in the active layer, for instance in figure 6.1, a sharp peak can often be observed at the point where h = 0 (and $\frac{\partial \eta}{\partial t}$ = 0). This may be due to the fact that equation (5.24) is not differentiable at this point and a switch from one part of this equation to the other occurs. This means that to the left of this point, where the sandwave is increasing, the active layer is filled with transported sediment, whereas right from this point, where the sandwave is eroding, the active layer is filled with sediment from the substrate.

For instance, from figure 6.1a, it can be observed that the concentration of the fine fraction on this point (where $h = 0$) , after two years tends to go from 0.2 to 0.9 in the increasing part and from a value of 0.5 to 0.9 in the eroding part, maybe causing the sharp peak. After 10 years, the concentration of the fine fraction on this point tends to go from 0 to 0.6 in the increasing part and from 0.5 to 0.6 in the eroding part. Therefore the peak is smaller here.

Attention should be given as well, to the fact that the results are only shown for the first ten years of the development of the sandwave. After that the graphs of the fractions gets pointed and peaked, and the results are no longer reliable. The sandwave still develops, but after about ten years, it is not only growing, but also changing its shape. This is shown in figure 6.5a. On the crest the sandwave is now eroding, whereas on the trough some sediment deposits. Due to this, more points are occur, where the model switches from erosion to deposition, or in other words, from one part of equation (5.24) to the other part. On these points again sharp peaks can occur, causing the unrealistic behaviour of the fractions after ten years.

7.1.2 The active layer thickness

The distribution of the fractions in the active layer evolves fast. Within a few years, only coarse grains are present in the active layer on the crest, whereas only fine grains are present in the active layer on the trough. The adaptation time of the system is influenced by the chosen active layer thickness. Sediment is transported in the horizontal direction, but the exchanging of the fractions in the active layer with the substrate is in the vertical direction. This vertical flux forms the dominating process, as the active layer is small compared with to the change in the bed level (Δh) and therefore a relative large part of the sediment in the active layer is exchanged each time step in comparison to the bed level change within a time step (For an explanation of time steps, see appendix 5). For instance on the crest of the sandwave, after two years of the reference simulation, the bed changed in the order of 0.0012m during one time step, which is more than the half of the active layer thickness, which is 0.002m. For the same time, the bottom changed on the trough with 0.0013m within one time step, which is even more. When comparing figure 6.8 with 6.10, the evolution of the fractions in the active layer seems indeed somewhat slower for a larger active layer.

In the trough of the sandwave hardly anything changes. This can also be explained from the active layer model. For the first 10 years, the part of the sandwave with positive height is continuously increasing and the part of the sandwave with negative height is continuously eroding (see figure 6.5). This means the sediment in the trough leaves the active layer and new sediment from the substrate is entrained. Therefore the active layer is continuously filled with sediment from the substrate with its own constant grain size distribution. Since the active layer is relatively small, most of the sediment is exchanged within one time step. Therefore after each time step, a value near the initial value of 0.5 is attained.

7.1.3 Hiding exposure

Finally, correcting for the hiding-exposure also influenced the system. When no hiding and exposure is taken into account, the development of the fractions seems to be faster. A hiding-exposure factor reduces the differences between the critical shear stresses of the grain sizes; this explains the differences between the behaviour of the fractions. Without this correction factor, the development of the fractions is more extreme and faster.

7.2 Discussion of the model results compared with field observations

In chapter 4, grain size data of 3 area's is discussed. In this chapter, the results obtained from the data of the area of sandwaves on a shoreface connected ridge near Zandvoort and the area 45 km west of Hoek van Holland, are compared with the model results. In the area that is situated 50 km offshore, no grain size sorting was visible. Therefore this area is not taken into account.

The model results show coarsening of the sandwave crest within a few years. After ten years, a percentage of 100% coarse sediment is in the active layer on the crest. The field observations show coarser grains on the crest as well (figure 4.6 and figure 4.10). However, in nature the sediment on the crest is only slightly coarser than in the trough. In the model however, no fine grains remain at the crest at all. The model results shows for the crest the same trend as observed by nature, but more extreme.

For the first years the model results show fine sediment on the slope, although in nature rather medium sediments (results from the sandwave field 50 km offshore, figure 4.10) or even coarse sediments (results from sandwave field 45 km offshore, figure 4.6) are found. This fining of the slopes however reduces after several years.
This reduction can caused by the fact that first the horizontal sediment flux accounts for both the growth of the sandwave and the exchange of the fractions. After some years the sandwave grows slower, but the sediment is still transported. Therefore the vertical sediment flux becomes larger and more important. Then the fine grains in the active layer are easier mixed with the coarse grains from the substrate. The sandwaves which are investigated for the field data are full-grown sandwaves. The model results however, show the development during the first ten years that the sandwave grows. Therefore the fining trend on the slope during the first few years cannot be validated with available data. After 10 years, the model results show no longer fine grains on the sandwave slope, which agrees with the field observations.

In the trough few changes occur during the first 10 years. This may be due to the model assumptions (see chapter 7.1.2). However, figure 6.4 show a little increase of the fine fractions in the active layer after 10 years. When the fine grains accumulated at the trough, this would agree with the findings in nature (figure 4.6 and 4.10).

When grain sizes are a bit coarser (figure 6.7), the evolution of the fractions is almost the same as for the reference run, only slower. When the grains are considerably coarser (figure 6.8), the model results show a different development of the grain size distribution in the active layer within the first few years. Fine grains accumulate at the crest and coarse grains at the slope. This can be caused by the fact that when grains are larger, fewer grains will go into transport and remain where they are. This can also explain why the accompanying sandwave has a slightly smaller length and height, in the case of very large grain sizes. When comparing the data of the area near Zandvoort (Appendix 2) and the area 45 km west of Hoek of Holland (Appendix 4), the latter also have some larger grain sizes than the area near Zandvoort. For the 45 km offshore area, the coarsest material can be found on the eastern slope, near the crest. However, the overall trend shows a coursing of sediment from trough to crest, in both areas. After 10 years, the grain size distribution of the model no longer shows differences for the greater grain sizes.

8. Conclusions

In this chapter some conclusions are given, answering the main research questions:

- When implementing heterogeneous sediment in an existing sandwave model, can this model made grain size sorting visible?
- If this is possible, how are the grains sorted over a sandwave?
- What is the influence of heterogeneous sediment on sandwave characteristics, compared with homogeneous sediment?
- Does the grain size sorting observed in nature agree with the model results?

To answer the first question, an existing sandwave model was extended with equations for heterogeneous sediment. This new model shows grain size sorting over sandwaves. The code seems to be suitable for the extension to heterogeneous sediment. Simulations can be done for the first ten years of the development of a sandwave, after that the results become unreliable.

For a bimodal mixture with grain sizes in the order of sediment in sandwave areas, a coarsening trend towards the sandwave crest is simulated, as well as a fining trend towards the slopes. This answers the second question. For larger grain sizes at first an opposite trend is simulated, but after 10 years the coarser grains accumulate on the crest again. The model simulates in both these cases hardly any sorting in the troughs. This might be a result of the used active layer model.

In order to answer the third question, simulations with heterogeneous sediment are compared with accompanying simulations with homogeneous sediment. No differences for sandwave characteristics are found, the sandwave length and height remain the same. Only for the case of large grains, the dimensions of the sandwave become smaller than in the reference case, as well for the heterogeneous as the homogeneous case. Therefore it can be said that the model shows no influence of heterogeneous sediment on the sandwave characteristics.

For the last question, data from TNO of three sandwave areas has been studied. It appears that in one area, with three dimensional sandwaves over a shoreface connected ridge, grain size sorting was found with a coarsening trend from the trough towards the crest. In a sandwave field 50 km offshore no grain size sorting seems to be present. On a sandwave in a sandwave field 45 km west of Hoek van Holland, grain size sorting was observed with a coarsening trend towards the eastern slope near the crest of the sandwave. These studied sandwaves were full-grown and therefore they should be compared best with the modelled grain size distribution after 10 years. The model shows also coarse grains on the sandwave crest. A fining trend towards the trough may start after 10 years, when the sandwave is growing slower. Therefore simulations of more then 10 years might be compared best with field observations.

In general, it can be said the model predicts grain size sorting processes which agree with field observations, although the processes are more extreme than in nature and are considerably influenced by the model assumptions.

9. Recommendations

Although grain size sorting can be modelled, there are still enough possibilities to improve this modelling. Also more investigation after the processes of grain size sorting can be done. In this chapter some recommendations for further research are discussed.

The transport equations which are used for this model are empirical and mostly based on river data. A more detailed research after the reliability of these equations would be preferable.

For this model the assumption was made that there are no other bedforms. In reality the sandwaves are often covered with megaripples. These smaller bedforms influence the sediment transport and the active layer thickness. To investigate this influence is recommended.

Also to treat the active layer thickness as a constant is not quite realistic. In reality it is possible, for instance, that there is a clay layer beneath the sandwave. After eroding in the trough, this non-erodible layer may be reached and than the active layer thickness becomes zero. Also when the sediment gets sorted, on the places with coarser sediment, the active layer is larger than on the places with finer sediment. A grain size dependent active layer thickness would overcome part of these problems.

Besides that, the complete active layer model turned out to be a strong simplification. To assume that the bottom consist of only two layers, the active layer and the substrate, causes unwanted behaviour of the fractions. A layer model with more layers, or another type of sediment continuity equation, may give a better prediction of the sorting processes.

Another assumption is the normal grain size distribution of the sediment. In the used equations the mean grain size is used, which is only suitable in case of normal distributed sediment. The measured samples from TNO however have only a near normal distribution and in reality the sediment has often a log-normal distribution. Also to take only two fractions into account is a simplification, although it gives a good insight in the processes. To simulate a realistic grain size distribution, more fractions should be necessary and equations for a log-normal distribution should be included in the model.

The fastest growing mode was found by simulating sandwave with different wavelengths with intervals of 50 meter. This gives only an approximation of the wavelength which will dominate the bed evolution. In order to find fastest growing mode in a correct way, each possible wavelength should be simulated. This would provide a more exact determined wavelength.

Wind waves are not included in this model. Therefore this model may be only valid for offshore regions, where the tidal flow is dominant. It is recommended to use this model with care in the (near-shore) regions were wind waves may influence the sediment transport.

The model includes only bed load transport. In reality sediment transport consist also of suspended load. This suspended load can also have a influence on the grain size sorting (McCave 1971, Walgreen 2003). Research from Van der Meer about the effect of homogeneous sediment in suspension at the sandwaves is ongoing. When it is possible, the extension to heterogeneous sediment in suspension may give a better insight in the total processes of grain size sorting.

It is also preferable to see what the effect of different grain sizes is on the sandwave characteristics. Therefore simulations with the code of all possible wavelengths must be made, to see which wavelength grow fastest and therefore dominates. Then the sandwave height and growth rate belonging to this wavelength can be found.

The last recommendation is that a detailed research of the behaviour of the fractions would be necessary to understand more about this behaviour. When on a certain moment the bottom and a shear stress profile over that bottom is given, the sediment equations and the equations belonging to the active layer, can be calculated for each point, to see what the fractions in first instance tends to do at that moment. Also the values of the sediment transport during a tidal cycle can be investigated. It is possible that, due to the critical shear stress, on a certain time during the low tide grains are not transported, whereas they are transported during high tide. To look at these intermediate values, instead of the total tidal averaged transport, creates a better insight in the different behaviour of grains with different sizes. These kinds of research would provide a better understanding of the sediment fraction behaviour.

References

Blondeaux, P., (2001), Mechanics of coastal forms, Annual. Rev. Fluid Mech, 33:339–70.

Blom, A. (2003). *A vertical sorting model for rivers with non-uniform sediment and dunes*, PhD thesis, University of Twente, The Netherlands.

Dodd, N., Blondeaux, P., Calvete, D., De Swart, H.E., Falqués, A., Hulscher, S.J.M.H., Różyński, G. and Vittori, G., (2003), *Understanding Coastal Morphodynamics Using Stability Methods*, Journal of Coastal Research.

Egiazaroff, I.V., (1965), Calculation of non-uniform sediment concentrations, *Journal of the hydraulics division*, ASCE, Vol. 91, No. 4, pp. 225-248.

Foti, E. and Blondeaux, P., (1995), Sea ripple formation: the heterogeneous sediment case*, Coastal Engineering* 25 237-253.

Hulscher, S.J.M.H. (1996). Tidal-induced large-scale regular bed form patterns in a three-dimensional shallow water model, *Journal of geophysical research*, vol. 101, no. C9, pages 20,727 - 20,744.

Kleinhans, M.G. (2002). *Sorting out sand and gravel: sediment transport and deposition in sand-gravel bed rivers*, PhD thesis, Utrecht University, The Netherlands.

Komarova, N.L. and Hulscher, S.J.M.H. (2000). Linear instability mechanisms for sand wave formation, *Journal of Fluid Mechanics,* vol. 413, pages 219-246.

Lanzoni, S. and Tubino, M., (1999), Grain sorting and bar instability, *J. Fluid Mech.* Vol. 393, pp. 149-174.

McCave, I.N.,(1971), Sand waves in the North Sea off the coast of Holland, *Marine Geology*, 10 (3), pp 199-225.

Meyer-Peter, E. and Müller, R., (1948), *Formulas for bed-load transport*, Proc. 2nd Congress IAHR, Stockholm, Sweden.

Németh, A.A. (2003). *Modelling offshore sand waves*, PhD thesis, University of Twente, The Netherlands.

Parker G. (2005). Morphodynamics e-book (http://www.cee.umn.edu/people/parkerg/morphodynamics_e-book)

Passchier, S. and Kleinhans M.G. (2005). Observations of sand waves, megaripples and hummocks in the Dutch coastal area and their relation ot currents and combined flow conditions, *Journal of Geophysical Research*, 110, F04S15, doi:10.1029/2004JF000215

Schüttenhelm, R.T.E. (2002). *Grain-size variability and crest stability of a North Sea sand wave in space and time,* TNO-report NITG 02-219-B, TNO, Utrecht, The Netherlands.

Seminara, G., (1995), *Effect* of grain sorting on the formation of bedforms, *Appl. Mech*. Rev. vol 48, no 9.

Soulsby, R., (1997). *Dynamics of marine sands,* Thomas Telford, England.

Tobias, C.J., (1989), *Morphology of sand waves in relation to current, sediment and wave data along the Eurogeul, North Sea,* report GEOPRO 1989.01; Dep. Of Physical Geography, University of Utrecht, The Netherlands.

Van den Berg, J. and Van Damme, R. M. J. (2005). Sand wave simulation on large domains, In Gary Parker & Garcia Marcello H. (Eds.), *River, Coastal and Estuarine Morphodynamics* (pp. 991-997). Leiden: Taylor & Francis / Balkema (ISBN 0-415-39376-0).

Van der Meer, F. M., Németh, A. A., and Hulscher, S. J. M. H. (2005), Modelling sand wave evolution using various sediment transport mechanisms, *Book of abstracts 5th International Conference on Coastal Dynamics 2005, 4-8 April 2005, Barcelona, Spain* (pp.404-405). Laboratori d'Enginyeri Marítima, Univ. Politèc. de Catalunya.

Van der Scheer, P., Ribberink, J.S. and Blom, A. (2002). *Transport formulas for graded sediment: behaviour of transport formulas and verification with data,* Research report CiT: 2002R-002, University of Twente, The Netherlands.

Van Dijk, T.A.G.P. (2002). *Geometry and patterns of bedforms in a coastal and shallow marine setting, North Sea,* TNO Report, Netherlands Institure of Applied Geosciences TNO, Utrecht, The Netherlands.

Van Dijk, T.A.G.P. and Kleinhans M.G. (2004). Processes controlling the behaviour of sandwaves and megaripples in the North Sea*, paper presented at Marine sandwave and river dune dynamics*, University of Twente, Enschede, The Netherlands.

Van Dijk, T.A.G.P. and Kleinhans M.G. (2005). Processing controlling the dynamics of compound sand waves in the North Sea, Netherlands, *Journal of Geophysical Research*, 110, F04S10, doi:10.1029/2004JF000173.

Van Rijn, L.C. (1993). *Principles of sediment transport in rivers, estuaries and coastal seas*. Aqua Publications, The Netherlands.

Walgreen, M., De Swart, H.E. and Calvete, D., (2003), Effect f grain size sorting on the formation of shoreface-connected sand ridges, *Journal of Geophysical Research*, 108, No.C3.

Walgreen, M., De Swart, H.E. and Calvete, D., (2004), A model for grain-size sorting over tidal sand ridges, *Ocean Dynamics* 54: 374-384.

Glossary

Active layer:	the topmost layer of the seabed that interacts with the flow on a single moment
Bedforms:	rhythmic wavelike patterns, on the bed of shallow seas
Bed load transport:	transportation of grains by rolling, hopping and sliding along the bed in response to friction and gravity (in the case of sloping beds)
Bimodal sediment:	sediment that consist of only two classes, each with its own grain size
Code:	translation of a model to a computer program (one model can have more than one code)
Crest:	top or topmost part, of the sandwave
Erosion:	lowering of the seabed due to sediment transport
Fastest growing mode:	wavelengths of the sandwave, which grows fastest (according to linear theory) and therefore are assumed to dominate the bed evolution
Fraction:	part of the sediment with its own specific grain size and concentration
Grain size:	diameter of a grain, a sediment particle (defined as the dimension of the smallest mesh opening through which the particle will pass or as the diameter of the equivalent sphere with the same fall velocity as the actual particle)
Heterogeneous sediment:	sediment which consists of grains with different grain sizes
Homogeneous sediment:	sediment which consist of grains with only one grain size
Mean:	averaged
Median:	midpoint in a distribution, value for which 50% of the distribution is larger and 50% is smaller
Model:	description or simplification of reality, expressed in mathematical equations

Sandwaves:	tidally induced, offshore bedforms consisting of sand, with wave heights in the order of meters to tens of meters and wavelengths in the order of hundreds of meters
Sandwave evolution:	the development of the sandwave
Sandwave height:	the difference between crest height and trough elevation
Sandwave growth:	the increasing height of a sandwave
Sandwave length:	the distance between the crests (or the troughs) of a sandwave
Sandwave migration:	movement of sandwaves from one place to another
Sediment:	in common: loose pieces of minerals and rock that can be transported by water, glaciers or wind; in this project: sand, non-cohesive material in the range 0.0625 to 2 mm
Sedimentation	deposition of sediment, when grains come to rest after transport, causing the sea bed to rise
Sediment transport:	displacement of grains due to the water motion
Slope:	flank of the sandwave, the incline between crest and trough
Sorting:	spatial variation of grain sizes over a sandwave; the converging of sediments with the same size on sandwave locations
Substrate:	the part of the seabed beneath the active layer, part of the sea bed that does not interact with the flow directly
Trough:	lower area between the sandwave crests

Appendix 1 Stability approach

Stability analysis

A morphodynamic system (a set of equations) describing the interaction between water motion and changing topography can be solved with a stability analysis, to explain the occurrence of certain patterns in the topography. Therefore first a basic state is defined, where these patterns are not present. This is in fact an equilibrium solution of the system (Dodd et al., 2003). The next step is to analyse what happens when small perturbations on this basic topography are superimposed. If all possible perturbations decay, the basic state is stable, but if there is at least one perturbation that grows, the basic state is unstable and bedforms will appear (Dodd et al., 2003).

Linear stability analysis

One possibility for the stability method is the linear stability analysis. When the solution of the problem is written as ψ and the basic state ψ_0 is perturbed by a small amplitude ε, this solution ψ can be expanded as follows:

$$\psi = \psi_0 + \varepsilon\psi_1 + \varepsilon^2\psi_2 + ...$$

The stability properties of the basic state can be investigated by determining the initial behaviour of ψ_1. When ε is small enough, the higher order terms can be left out of consideration, which is called a linear stability analysis (Németh, 2003). This gives a good approximation only for the initial evolution of the bedforms. The perturbations will now have exponentially decaying or growing amplitudes, which can be quantified in a negative or positive growth rate, respectively. The perturbation with the largest growth rate will prevail after some time (Dodd et al., 2003). This is called the fastest growing mode (FGM).

Information of the bedforms that can be obtained from a linear stability analysis are the preferred wavelength, the shape (i.e., elongated, rounded, shore-normal, orientation with respect to the periodic direction etc.), the growth rate and the migration rate (Dodd et al., 2003).

Appendix 2 Sandwaves on shoreface-connected ridge, Zandvoort

In table 1 the selected grain size data of sea bed samples for the sandwaves on shoreface-connected ridge near Zandvoort, in March 2001 are shown; D_{10}, D_{50}, D_{60}, D_{90} with grain sizes in µm, uniformity coefficient D_{60}/D_{10}, water depth in dm, the morphologic description and the NITG sample numbers, corresponding to figure 1.

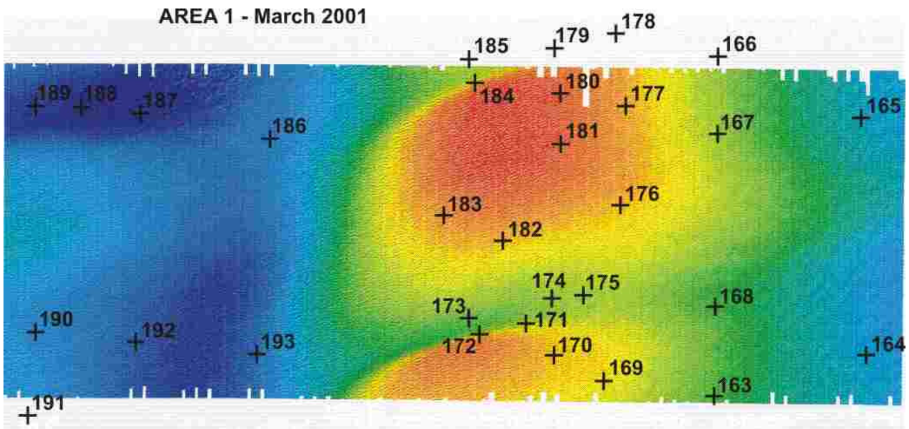

Figure 1: Coastal site with sample locations on 3D sandwaves on a shoreface-connected ridge near Zandvoort.

NITG nr.	d (0.1)	d (0.5)	d (0.6)	d (0.9)	d60/d10	morphologic description	water depth (dm)
163	262.56	366.11	391.29	508.14	1.490297	vlak gebied ZO, dichtbij bank	160
166	257.07	356.12	380.34	493.50	1.479538	vlak gebied ZO, dichtbij bank	156
167	256.51	354.16	378.04	489.88	1.473768	vlak gebied ZO, dichtbij bank	155
168	254.81	352.46	376.39	488.56	1.477149	vlak gebied ZO, dichtbij bank	160
169	257.59	359.58	384.53	500.88	1.492779	flauwe ZO helling van bank	151
170	253.99	352.03	376.02	488.12	1.480456	top van bodemvorm	148
180	247.20	341.78	364.89	472.88	1.476064	top van bodemvorm	144
181	254.14	351.12	374.85	485.66	1.474996	top van bodemvorm	144
183	243.32	336.16	359.01	467.68	1.475476	steile W-helling van bank	146
184	233.21	322.88	344.79	446.52	1.478455	steile N-helling van bodemvorm	150
173	229.68	319.40	341.29	442.48	1.485889	tussen de bodemvormen	158
185	231.52	321.26	343.17	444.86	1.482231	tussen de bodemvormen	154
189	209.37	299.59	322.13	428.61	1.538532	laaggelegen gebied NW	181
190	215.07	308.07	331.36	441.43	1.540699	laaggelegen gebied NW	174
191	216.05	310.32	334.02	446.96	1.546001	laaggelegen gebied NW	173

Table 1: Selected grain size data of sea bed samples for the sandwaves on a shoreface-connected ridge in March 2001, grain sizes in [µm], water depth in [dm] and NITG sample numbers correspond to the figure above.

Appendix 3 Sandwave field in offshore area

Table 2 shows the selected grain size data of sea bed samples for the offshore sandwave field, corresponding to figure 2.

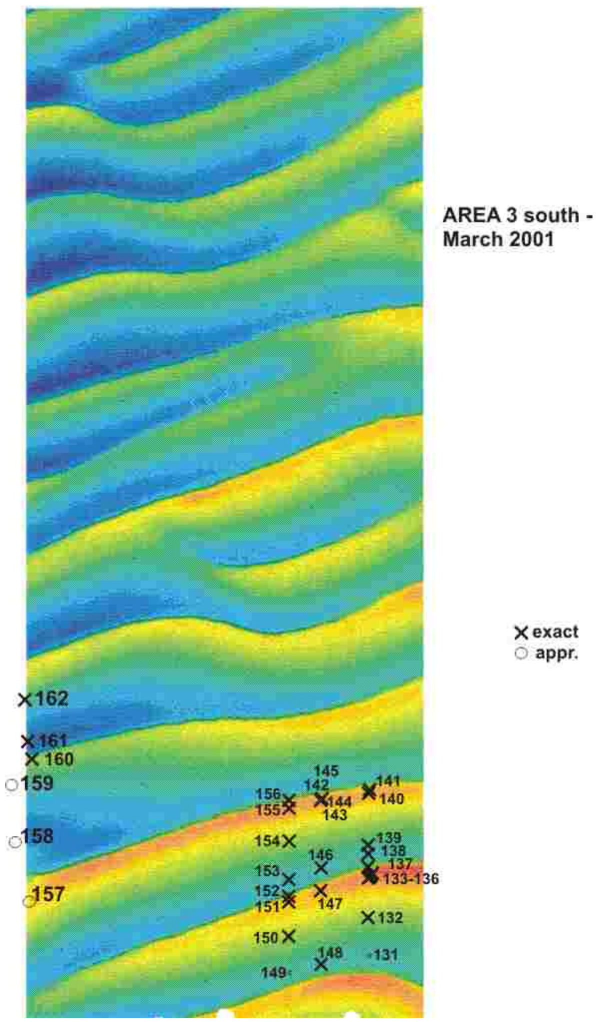

Figure 2: 2D sandwaves field, 50 km offshore Egmond

NITG nr.	d (0.1)	d (0.5)	d (0.6)	d (0.9)	d60/d10	morphologic description	water depth (dm)
131	203.09	281.98	301.32	392.76	1.48368	zandgolf trog	282
138	202.88	282.17	301.61	393.67	1.486669	zandgolf trog	283
149	206.51	286.35	306.03	399.54	1.481921	zandgolf trog	282
153	198.97	276.80	295.82	384.40	1.486709	zandgolf trog	283
158	196.77	274.30	293.23	381.04	1.490194	zandgolf trog	292
162	213.92	297.91	318.55	416.00	1.489094	zandgolf trog	280
140	199.96	277.74	296.74	385.33	1.483987	zandgolf top	266
151	205.28	284.74	304.27	396.69	1.482178	zandgolf top	267
155	207.77	287.84	307.56	401.44	1.480307	zandgolf top	263
157	205.35	284.65	304.13	396.28	1.480998	zandgolf top	268
160	218.61	303.58	324.46	422.96	1.4842	zandgolf top	276

Table 2: Selected grain size data of sea bed samples for the offshore sandwave field in March 2001, grain sizes in [µm], water depth in [dm] and NITG sample numbers correspond to the figure above.

Appendix 4 Sandwaves field, 45 km west of Hoek van Holland

The grain size data of sample points at the first 5 cm of the bottom, for the Sandwave field, 45 km west of Hoek van Holland, are shown in table 3. For the location of these sample points see figure 3.

Location	d50 [µm]	d60/d10 [-]
11	390	1.55
10	410	1.62
9	420	1.61
8	506	1.63
4	414	1.61
5	405	1.55
6	382	1.63
7	450	1.55
4	414	1.61
3	405	1.62
2	393	1.54
1	399	1.55
12	408	1.55
13	561	1.77
14	411	1.64
16	396	1.63
19	303	1.80
18	364	1.54
17	457	1.63
16	396	1.63
20	370	1.63
21	375	1.63
22	432	1.73
23	461	1.75

Table 3: Selected grain size data of sea bed samples for the Sandwave field, 45 km west of Hoek van Holland in April 2001, grain sizes in [µm], and sample numbers correspond to the figure beneath.

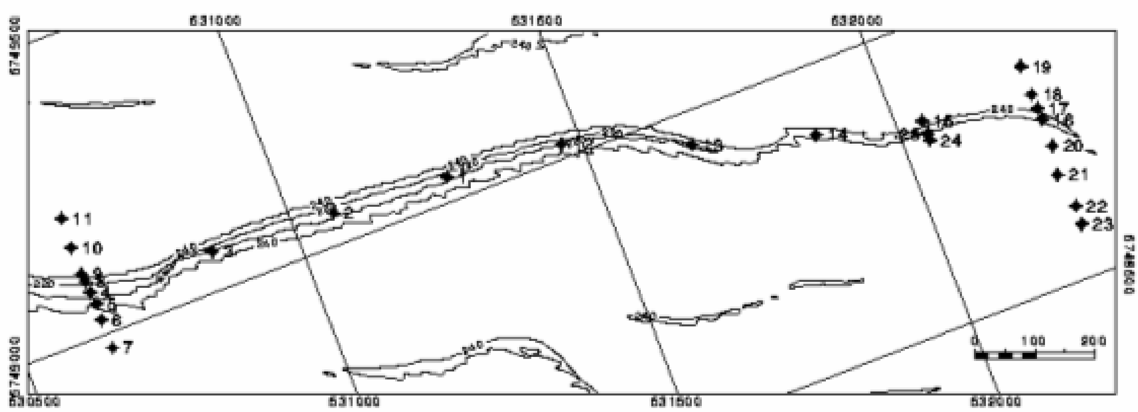

Figure 3: Location map of short cores, scales in meters.

Appendix 5 Technical details for the numerical calculation

In this appendix an explanation is given how the new equations are implemented in the code.

For the numerical calculations, the length of the sandwave is divided into intervals which all have the same length Δx. For each point n * Δx, the equations can be solved. The same is done for the time. The time is divided into time-intervals, or time steps, which all have the same size Δt. The time-dependant equations are solved for each moment after a time step Δt.

First D_m is calculated for each point and time (with equation (5.16)). With the help of this value D_m, for each point the critical shear stress is determined (using equation (5.15) and then (5.14)). Finally the transport rate for each fraction is calculated for each point and time (equation (5.23), with the help of the parameters of equation (5.17), (5.20) and (5.22)). Then all these values of sediment transport rate for every time step are summed and finally the sum is divided by the total amount of time steps, to get the tidal averaged sediment transport rate for each point.

Now the active layer model can be solved. Because δ is constant, equations (5.24) and (5.26) can with the help of equation (5.27), can be written as:

$$c_b \delta \frac{\partial F_i}{\partial t} + c_b F_{Ii} \frac{\partial h}{\partial t} = -\frac{\partial q_i}{\partial x} \tag{0.1}$$

and

$$c_b \frac{\partial h}{\partial t} = -\frac{\partial \sum_i q_i}{\partial x}. \tag{0.2}$$

First the transport ratios for all fractions are summed up, to get the total amount of sediment, q_{tot}. Equation (0.2) than becomes:

$$c_b \frac{\partial h}{\partial t} = -\frac{\partial q_{tot}}{\partial x}. \tag{0.3}$$

This equation can discretized as follows:

$$c_b \frac{\Delta h}{\Delta t} = -\frac{\Delta q_{tot}}{\Delta x} = -\frac{q_{tot}{}^{n} - q_{tot}{}^{n-1}}{\Delta x}, \tag{0.4}$$

in which n is the number of the x-point.
From this equation, Δh can be solved:

$$\Delta h = -\frac{1}{c_b} \frac{\Delta t}{\Delta x} (q_i - q_{i-1}). \tag{0.5}$$

Then the bottom height at the next time level, h_{new}, can be calculated from the old bottom state, h_{old}, with:

$$h_{new} = h_{old} + \Delta h. \tag{0.6}$$

From Δh it is known which F_{Ii} must be used in equation (0.1) (See also equation (5.24)).

In the case that $\Delta h > 0$, this equation becomes:

$$c_b \delta \frac{\partial F_i}{\partial t} + c_b F_{i,old} \frac{\partial h}{\partial t} = -\frac{\partial q_i}{\partial x} . \qquad (0.7)$$

In discrete form this becomes:

$$c_b \delta \frac{\Delta F_i}{\Delta t} + c_b F_{i,old} \frac{\Delta h}{\Delta t} = -\frac{\Delta q_i}{\Delta x} = \frac{q_i^{\,n} - q_i^{\,n-1}}{\Delta x} . \qquad (0.8)$$

From this equation ΔF_i can be solved:

$$\Delta F_i = -\frac{1}{\delta} F_{i,old} \Delta h - \frac{1}{\delta c_b} \frac{\Delta t}{\Delta x} (q_i^{\,n} - q_i^{\,n-1}) . \qquad (0.9)$$

For $F_{i,old}$, the value from F_i, calculated in the previous loop, is taken. This is an explicit method.

In the case that $\Delta h < 0$, equation (0.1) becomes:

$$c_b \delta \frac{\partial F_i}{\partial t} + c_b F_s \frac{\partial h}{\partial t} = -\frac{\partial q_i}{\partial x} . \qquad (0.10)$$

Numerically this can be written as:

$$c_b \delta \frac{\Delta F_i}{\Delta t} + c_b F_s \frac{\Delta h}{\Delta t} = -\frac{\Delta q_i}{\Delta x} = \frac{q_i^{\,n} - q_i^{\,n-1}}{\Delta x} . \qquad (0.11)$$

As F_s has a constant value, from this equation ΔF_i can be solved:

$$\Delta F_i = -\frac{1}{\delta} F_s \Delta h - \frac{1}{\delta c_b} \frac{\Delta t}{\Delta x} (q_i^{\,n} - q_i^{\,n-1}) . \qquad (0.12)$$

Now the new value for the fraction, $F_{i,new}$, can be calculated:

$$F_{i,new} = F_{i,old} + \Delta F_i . \qquad (0.13)$$

With this new value of the fraction, the new sediment transport rate can be calculated. This is done in an explicit way.